Pergamon

Int. J. Heat Mass Transfer. Vol. 37, No. 15, pp. 2343–2365, 1994

0017–9310/94 $7.00 + 0.00

0017–9310(94)E0025–P

Mixed convection from a straight isothermal tube of elliptic cross-section

H. M. BADR

Mechanical Engineering Department, King Fahd University of Petroleum and Minerals, Dhahran 31261, Saudi Arabia

(*Received* 17 *February* 1993)

Abstract—The problem of laminar mixed (natural and forced) convective heat transfer from a straight isothermal tube of elliptic cross-section placed in a uniform stream is investigated. The free stream direction is horizontal and normal to the tube axis and the flow field is essentially two-dimensional. The investigation is based on a numerical solution of the conservation equations of mass, momentum, and energy. The resulting velocity and thermal fields both are found to be either steady or quasi-steady depending on vortex shedding. The parameters involved are the Reynolds number, Re, Grashof number, Gr, Prandtl number, Pr, the tube geometry represented by its axis ratio (minor to major), A_r, and its orientation represented by its angle of inclination, λ. The study focuses on the effects of Re, Gr, and λ on the heat transfer process in the Re range from 20 to 500, Gr range from 0 to 1.25×10^6 and for angles of inclination varying from 0° to 180°. The average Nusselt number is found to increase considerably with the increase of the ratio Gr/Re^2. The response of the total rate of heat transfer to changes in the inclination angle is found to depend on the Reynolds number. The results also indicate that the increase of Gr for a given value of Re tends to suppress vortex shedding. The details of the velocity and thermal fields are presented in the form of isotherm and streamline patterns in addition to the surface vorticity and local Nusselt number distributions.

1. INTRODUCTION

HEAT transfer from elliptic cylinders has been the subject of many experimental investigations because of its numerous engineering applications. Heat exchangers made of tubes of circular cross-section are commonly used in industry. However, flow over these tubes is not always perpendicular to the tube axis which makes the tube cross-section in the direction of flow to have an elliptic shape. In general, the elliptic tube geometry can represent the circular tube and can also represent a very thin plate depending on the value of the axis ratio. The overall heat transfer from an elliptic tube depends on its geometry (i.e. axis ratio, surface roughness, and angle of attack), the fluid properties, the approaching flow condition, and the tube surface temperature distribution. In general, various heat transfer modes may take place ranging from forced convection dominated regime to free convection dominated one. Combined (free and forced) heat transfer mode may also take place when inertia and buoyancy forces are comparable. The local heat transfer features for an elliptic tube set normal to an approaching free stream differs considerably from that of a circular tube. The heat transfer characteristics are strongly influenced by the axis ratio, the angle of attack, and the Reynolds and Grashof numbers.

The characteristics of steady asymmetrical flow over cylinders in the absence of buoyancy forces was the subject of many theoretical studies. The problem of 2-D flow past an elliptic cylinder at different angles of attack was investigated theoretically in the low Reynolds number range by many researchers [1–6]. Several researchers have investigated both experimentally and theoretically the time development of the flow field adjacent to an elliptic cylinder starting its motion from rest. This problem is of fundamental importance since the flow field is unsteady for a considerable range of Reynolds number due to vortex shedding. Various approaches have been utilized for tackling this problem. For example, Izumi *et al.* [7] used a discrete-vortex simulation model to predict the vortex formation in the wake. In this model, a number of vortices were introduced in the flow and then convected downstream in order to simulate the vortex shedding process. The same problem was studied by Daube *et al.* [8] for the case of an elliptic cylinder starting its motion impulsively in a fluid at rest. The analysis was based on a numerical integration of the unsteady Navier–Stokes equations using finite-differences. Results were obtained for a Reynolds number of 10^3 and for an angle of attack of 30°: however, neither steady nor quasi-steady flow fields were achieved. The case of a uniformly accelerated thin elliptic cylinder moving normal to its axis in a viscous fluid was studied by Tanahashi *et al.* [9] who solved the vorticity transport equation to simulate numerically the initial stage of flow development near the cylinder. Results were obtained for the variation of the lift, drag, and moment coefficients during a short time period following the start of the cylinder motion. In their study, the angle of attack was varied from 15° to 90°, however, the only Reynolds number considered was 98.11.

NOMENCLATURE

A_r axis ratio, b/a
a, b semi-major and minor axes
c focal distance
F_0, f_n, F_n functions defined in equation (7a)
g gravitational acceleration
G_0, g_n, G_n functions defined in equation (7b)
Gr Grashof number, $g\beta(T_s - T_\infty)(2c)^3/\nu^2$
h heat transfer coefficient
H_0, h_n, H_n functions defined in equation (7c)
k fluid conductivity
Nu local Nusselt number
$\overline{Nu}$ average Nusselt number
$\overline{Nu}_f$ average Nusselt number for forced convection
p fluid pressure
Pe Peclet number, $Re\,Pr$
Pr Prandtl number, ν/α
Re Reynolds number, $2u_\infty c/\nu$
t dimensionless time
T fluid temperature
u, v velocities in x- and y-directions, respectively
x, y rectilinear coordinates
z boundary-layer coordinate.

Greek symbols
α thermal diffusivity
β coefficient of volumetric thermal expansion
ζ vorticity
η, ξ elliptical coordinates
λ angle of inclination of the tube
ν kinematic viscosity
ρ density
ϕ dimensionless temperature
Ψ stream function.

Subscripts
0 at the surface
∞ at infinite distance from the surface.

Experimental investigations of the characteristics of the flow field adjacent to an elliptic cylinder are numerous [10–15]. A good survey of the experimental work done on this problem up to 1987 is given in the paper by Ota *et al.* [16]. In that paper, an experimental study was carried out on the problem of flow over an elliptic cylinder of axis ratio of 1 : 3 in the critical Reynolds number range of 3.5×10^4–1.25×10^5 (based on the major axis length). The study revealed that the critical Reynolds number depends on the angle of attack and attains a minimum value when the angle is between 5° and 10°. It was also found that a small separation bubble exists near the leading edge in the critical Reynolds number regime.

Although published research on convective heat transfer from elliptic cylinders shows a good number of experimental investigations, it is only limited to forced convection problems. To the best of the author's knowledge, the first measurements of the local heat transfer coefficient were reported in 1953 by Seban and Drake [17] and by Drake *et al.* [18] who conducted their experimental studies for cylinders of axis ratio 1 : 4 and 1 : 3, respectively. The study was limited to forced convection regime and small angles of attack (0°, 5°, and 6° only). In 1983, Ota *et al.* [19, 20] reported their experimental results on forced convection from elliptic cylinders of axis ratios of 1 : 2 and 1 : 3 placed in a uniform stream in the Reynolds number range of 5×10^3–9×10^4 and for angles of attack varying from 0° to 90°. The variation of the local heat transfer coefficient was found, as expected, to be quite different from that of a circular cylinder. In addition, the angle of attack was found to have a strong influence on the overall heat transfer rate. It was also found that the angle of attack producing the minimum average heat transfer coefficient depends on the Reynolds number range. No attempt was made to study the effect of the interaction between buoyancy driven flow and forced flow on the overall heat transfer rate.

Recently (1988) Nishiyama *et al.* [21, 22] published their findings on the problem of convective heat transfer from elliptic cylinders placed in tandem arrangements. The study is purely experimental and was conducted once for two cylinders and again for four cylinders of axis ratio 1 : 2 in both cases. Local and average heat transfer characteristics were presented for various angles of attack ranging from 30° to 60° for the case of two cylinders and from 0° to 90° for the case of four cylinders. In their work they focused on forced convection regime only. Another recent work (1988) on this problem is that carried out by Ilgarubis *et al.* [23] who investigated the drag and heat transfer characteristics of compact bundles of elliptical finned tubes. They focused on the variation of the average heat-transfer coefficient from one row to another. The investigation covered the Reynolds number range from 4×10^2 to 4×10^3.

Theoretical studies of convective heat transfer from elliptic cylinders are very few and are all based on the solution of boundary-layer equations. The works by Eckert [24] and by Chao and Fagbenle [25] are mainly boundary-layer analyses for the forced convection heat transfer problem. According to the boundary-layer approximations, their results are only applicable in the neighborhood of the leading edge where the

boundary-layer thickness is small. As the angle of attack increases, one would expect flow separation to occur earlier on the upper surface and accordingly the region of validity of the boundary-layer solution gets smaller. The only boundary-layer analysis of free convection from elliptic cylinders was reported by Merkin [26] who solved the boundary-layer equations for the case of buoyancy-driven flow over an elliptic cylinder for the two cases in which the major axis is either horizontal or vertical. Although it was pointed out that the boundary-layer model will not be appropriate in the immediate vicinity of the top of the cylinder, the numerical integration continued, reaching that point because of the absence of flow separation. As a result, one may conclude that the boundary-layer model cannot be utilized to study the entire flow field in either case of forced or combined convection regimes since flow separation in most of these cases is unavoidable.

According to the above literature review, it is clear that there no attempt has been made to tackle the problem of combined (free and forced) convection heat transfer form an elliptic cylinder either theoretically or experimentally. The only theoretical investigation of the problem of forced convection is based on the solution of the boundary-layer equations which are valid only in the neighborhood of the leading edge. No attempt has been made to study the entire flow field based on the full conservation equations of mass, momentum and energy. This work aims to conduct a theoretical study of combined convection from an elliptic cylinder set normal to an approaching free stream at various angles of attack. The study is based on solving the conservation equations of mass, momentum (Navier–Stokes equations), and energy. Detailed analysis of the flow and thermal fields adjacent to the cylinder surface are carried out. The effects of Reynolds number, Grashof number, and the angle of attack on the local and average heat transfer coefficients are studied for cylinders of axis ratios $A_r = 0.6$.

2. PROBLEM STATEMENT AND GOVERNING EQUATIONS

The problem considered is that of mixed (forced and natural) convection heat transfer from a straight tube of elliptic cross-section with $2a$ and $2b$ representing the major and minor axes, respectively. The tube, which has an isothermal outer surface of temperature T_s, is placed horizontally normal to a uniform stream of velocity u_∞ and temperature T_∞. The major axis of the tube cross-section may be horizontal or inclined at an angle λ as shown in Fig. 1. The flow field is assumed laminar, two-dimensional (neglecting end effects) and unsteady. The flow unsteadiness arises essentially from vortex shedding. Applying the Boussinesq approximation and neglecting viscous dissipation, the governing equations of motion and energy can be expressed as:

$$\frac{\partial\zeta}{\partial t}+u\frac{\partial\zeta}{\partial x}+v\frac{\partial\zeta}{\partial y}=\frac{2}{Re}\nabla^2\zeta - \frac{Gr}{2Re^2}\left[\cos\lambda\frac{\partial\phi}{\partial x}+\sin\lambda\frac{\partial\phi}{\partial y}\right], \quad (1)$$

$$\zeta=\nabla^2\psi, \quad (2)$$

$$\frac{\partial\phi}{\partial t}+u\frac{\partial\phi}{\partial x}+v\frac{\partial\phi}{\partial y}=\frac{2}{Re\,Pr}\nabla^2\phi, \quad (3)$$

where t is the time, u and v are the velocity components in the x- and y-directions, ψ is the stream function, ζ is the vorticity, ϕ is the temperature, Gr is the Grashof number, Re is the Reynolds number, and Pr is the Prandtl number. All the above variables are dimensionless and related to the dimensional quantities by:

$$x=\frac{x'}{c}\quad y=\frac{y'}{c}\quad u=\frac{u'}{u_\infty}\quad v=\frac{v'}{u_\infty}$$

$$t=\frac{u_\infty t'}{c}\quad \phi=\frac{T-T_\infty}{T_s-T_\infty}\quad \psi=\frac{\psi'}{cu_\infty}\quad \zeta=-\frac{\zeta' c}{u_\infty},$$

where $c=(a^2-b^2)^{1/2}$ is the focal distance and all the variables with primes are dimensional in addition to the temperature T. The Grashof and Reynolds numbers are defined as:

$$Re=\frac{2u_\infty c}{\nu}\quad Gr=\frac{g\beta(2c)^3(T_s-T_\infty)}{\nu^2},$$

where g is the gravitational acceleration, β is the coefficient of volumetric thermal expansion, and ν is the kinematic viscosity.

Since the elliptic coordinates (ξ,η) are more appropriate for use in the present problem, we now use the transformation:

$$x=c\cosh\xi\cos\eta\quad y=c\sinh\xi\sin\eta,$$

with $\xi_0=\tanh^{-1}(A_r)$ defining the outer surface of the tube.

Using the above transformation, the governing equations (1–3) can be expressed as:

$$H\frac{\partial\zeta}{\partial t}+\frac{\partial\psi}{\partial\eta}\frac{\partial\zeta}{\partial\xi}-\frac{\partial\psi}{\partial\xi}\frac{\partial\zeta}{\partial\eta}=\frac{2}{Re}\nabla^2\zeta - \frac{Gr}{2Re^2}\left[\frac{\partial\phi}{\partial\xi}(\cosh\xi\sin\eta\sin\lambda+\sinh\xi\cos\eta\cos\lambda) - \frac{\partial\phi}{\partial\eta}(\cosh\xi\sin\eta\cos\lambda-\sinh\xi\cos\eta\sin\lambda)\right], \quad (4)$$

$$H\zeta=\nabla^2\psi \quad (5)$$

$$H\frac{\partial\phi}{\partial t}+\frac{\partial\psi}{\partial\eta}\frac{\partial\phi}{\partial\xi}-\frac{\partial\psi}{\partial\xi}\frac{\partial\phi}{\partial\eta}=\frac{2}{Pe}\nabla^2\phi, \quad (6)$$

where

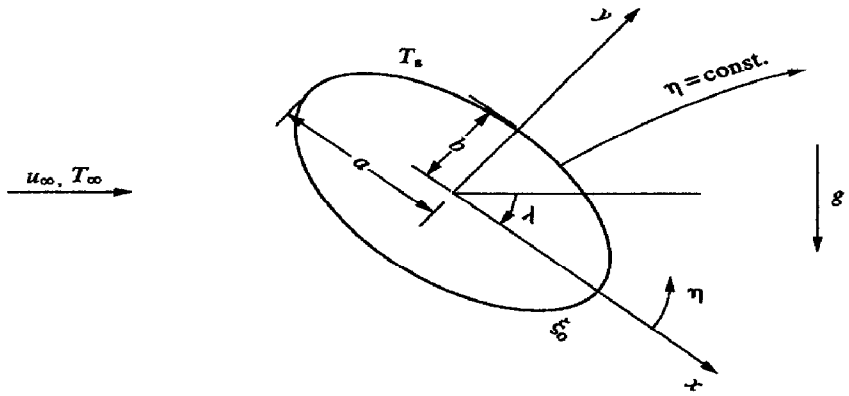

FIG. 1. The elliptic section geometry and the coordinate systems.

$$\nabla^2 = \frac{\partial^2}{\partial \xi^2} + \frac{\partial^2}{\partial \eta^2}, \quad H = \tfrac{1}{2}(\cosh 2\xi - \cos 2\eta),$$

and $Pe = Re\,Pr$ is the Peclet number.

The boundary conditions of the velocity field are mainly the no slip and impermeability conditions on the tube surface and the free stream conditions far away from it. These conditions can be expressed as:

$$\psi = \frac{\partial \psi}{\partial \xi} = \frac{\partial \psi}{\partial \eta} = 0 \quad \text{when } \xi = \xi_0,$$

and:

$$\left.\begin{aligned} &\zeta \to 0 \\ &\frac{\partial \psi}{\partial \xi} \to -\frac{1}{2} e^{\xi} \sin(\lambda - \eta) \\ &\frac{\partial \psi}{\partial \eta} \to \frac{1}{2} e^{\xi} \cos(\lambda - \eta) \end{aligned}\right\} \quad \text{as } \xi \to \infty.$$

The thermal field boundary conditions are simply the constant temperature on the tube surface and the free stream temperature far away. These can be written as:

$$\phi = 1 \quad \text{when} \quad \xi = \xi_0 \quad \phi \to 0 \quad \text{as } \xi \to \infty.$$

3. THE METHOD OF SOLUTION

In the present problem, the velocity and thermal fields may be unsteady due to the formation of vortices near the tube surface and its shedding downstream. Accordingly, the method of solution is constructed to solve the time dependent problem in order to predict the time variation of both velocity and thermal fields. The method is based on numerical integration of the governing equations (4)–(6) in space and time starting from certain initial conditions until eventually reaching a steady or quasi-steady state. The time development of the flow and thermal fields is carried out in two stages. In the first stage, the free stream is assumed to start suddenly from rest with no temperature difference between the tube surface and the approaching stream (i.e. in the absence of buoyancy forces). At the beginning of this stage, the boundary-layer region starts to form in the immediate neighborhood of the tube surface and then grows with time. Later on, when the boundary layer becomes thick enough, the tube temperature is suddenly and uniformly increased to T_s allowing both thermal and velocity fields to develop simultaneously with time. The method is similar to that used by Badr [27]. In order to decrease the number of independent variables the functions ψ, ζ, and ϕ are approximated using Fourier series as follows:

$$\psi = \frac{1}{2}F_0(\xi, t) + \sum_{n=1}^{N} f_n(\xi, t) \sin n\eta + F_n(\xi, t) \cos n\eta, \tag{7a}$$

$$\zeta = \frac{1}{2}G_0(\xi, t) + \sum_{n=1}^{N} g_n(\xi, t) \sin n\eta + G_n(\xi, t) \cos n\eta, \tag{7b}$$

$$\phi = \frac{1}{2}H_0(\xi, t) + \sum_{n=1}^{N} h_n(\xi, t) \sin n\eta + H_n(\xi, t) \cos n\eta, \tag{7c}$$

where N is the number of terms in the Fourier series.

To obtain a separate equation for each of the functions G_0, g_n, and G_n, we substitute the above expressions of ψ, ζ, and ϕ in equation (4) and, by using simple mathematical manipulation, we obtain:

$$\frac{1}{2}\cosh 2\xi \frac{\partial G_0}{\partial t} - \frac{1}{2}\frac{\partial G_2}{\partial t} = \frac{2}{Re}\frac{\partial^2 G_0}{\partial \xi^2} + s_{n0}(\xi, t), \tag{8a}$$

$$\cosh 2\xi \frac{\partial g_n}{\partial t} - \frac{1}{2}\operatorname{sgn}(n-2)\frac{\partial g_{|n-2|}}{\partial t} - \frac{1}{2}\frac{\partial g_{n+2}}{\partial t} = \frac{4}{Re}\left[\frac{\partial^2 g_n}{\partial \xi^2} - n^2 g_n\right] + s_{n1}\left[\xi, t, \lambda, \frac{Gr}{2Re^2}\right], \tag{8b}$$

$$\cosh 2\xi \frac{\partial G_n}{\partial t} - \frac{1}{2}\left[\delta_{n2}\frac{\partial G_0}{\partial t} + \frac{\partial G_{|n-2|}}{\partial t} + \frac{\partial G_{n+2}}{\partial t}\right] = \frac{4}{Re}\left(\frac{\partial^2 G_n}{\partial \xi^2} - n^2 G_n\right) + s_{n2}\left(\xi, t, \lambda, \frac{Gr}{2Re^2}\right), \tag{8c}$$

where

$$\delta_{mn} = \begin{cases} 1 & \text{when } n = m \\ 0 & \text{when } n \neq m \end{cases},$$

$\mathrm{sgn}(n-2)$ represents the sign of the term $(n-2)$, and the terms $g_{|n-2|}$ and $G_{|n-2|}$ in equations (8b) and (8c) vanish when $n = 2$. The functions s_{n0}, s_{n1}, and s_{n2} can be easily identified. Equation (8) defines a set of $(2N+1)$ differential equations to be integrated in time in order to advance the solution of G_0, g_n, and G_n through one time step.

We also substitute from equations (7a) and (7b) in equation (5) and integrate both sides of the resulting equation (after multiplying each side, once at a time by 1, $\sin n\eta$, $\cos n\eta$) with respect to η between the limits 0 and 2π to obtain:

$$\frac{\partial^2 F_0}{\partial \xi^2} = \frac{1}{2}(\cosh 2\xi)\, G_0 - \frac{1}{2} G_2, \tag{9a}$$

$$\frac{\partial^2 f_n}{\partial \xi^2} - n^2 f_n = \tfrac{1}{2}(\cosh 2\xi) g_n - \tfrac{1}{4}[\mathrm{sgn}(n-2) g_{|n-2|} + g_{(n+2)}], \tag{9b}$$

$$\frac{\partial^2 F_n}{\partial \xi^2} - n^2 F_n = \tfrac{1}{2}(\cosh 2\xi) G_n - \tfrac{1}{4}[\delta_{n2} G_0 + G_{|n-2|} + G_{(n+2)}]. \tag{9c}$$

Equation (9) defines another set of $(2N+1)$ differential equations relating the Fourier components of the stream function to the corresponding components of the vorticity. A third set of differential equations can be obtained by using equations (7a) and (7c) together with equation (6) and following the same steps used in deriving equation (9), we finally obtain:

$$\frac{1}{2}\cosh 2\xi \frac{\partial H_0}{\partial t} - \frac{1}{2}\frac{\partial H_2}{\partial t} = \frac{2}{Pe}\frac{\partial^2 H_0}{\partial \xi^2} + Z_{n0}(\xi, t), \tag{10a}$$

$$\cosh 2\xi \frac{\partial h_n}{\partial t} - \frac{1}{2}\mathrm{sgn}(n-2)\frac{\partial h_{|n-2|}}{\partial t} - \frac{1}{2}\frac{\partial h_{n+2}}{\partial t} = \frac{4}{Pe}\left(\frac{\partial^2 h_n}{\partial \xi^2} - n^2 h_n\right) + Z_{n1}(\xi, t), \tag{10b}$$

$$\cosh 2\xi \frac{\partial H_n}{\partial t} - \frac{1}{2}\left(\delta_{n2}\frac{\partial H_0}{\partial t} + \frac{\partial H_{|n-2|}}{\partial t} + \frac{\partial H_{n+2}}{\partial t}\right) = \frac{4}{Re}\left(\frac{\partial^2 H_n}{\partial \xi^2} - n^2 H_n\right) + Z_{n2}(\xi, t). \tag{10c}$$

Equations (10a)–(10c) define a third set of $(2N+1)$ differential equations to be used for advancing the thermal field in time. The functions Z_{n0}, Z_{n1}, and Z_{n2} are easily identifiable.

The boundary conditions for all the functions (Fourier coefficients) can be obtained by using equations (7a)–(7c) together with the known boundary conditions for ψ, ζ, and ϕ written following equation (6). These can be expressed as:

$$H_0 = 2$$

$$h_n = H_n = F_0 = f_n = F_n = \frac{\partial}{\partial \xi}(F_0, f_n, F_n) = 0 \quad \text{when } \xi = \xi_0, \tag{11a}$$

$$H_0, h_n, H_n, G_0, g_n, G_n, F_0, \frac{\partial F_0}{\partial \xi} \Rightarrow 0 \quad \text{as } \xi \Rightarrow \infty, \tag{11b}$$

$$\left.\begin{aligned} \frac{\partial f_n}{\partial \xi} &\Rightarrow \frac{1}{2}\delta_{n1}\, e^{\xi}\cos\lambda \\ \frac{\partial F_n}{\partial \xi} &\Rightarrow -\frac{1}{2}\delta_{n1}\, e^{\xi}\sin\lambda \end{aligned}\right\} \quad \text{as } \xi \Rightarrow \infty. \tag{11c}$$

A set of integral conditions are also obtained by integrating both sides of each of equations (9a)–(9c) and applying the boundary conditions given in equation (11). These conditions can be written as:

$$\int_{\xi_0}^{\infty} [(\cosh 2\xi) G_0 - G_2]\, d\xi = 0, \tag{12a}$$

$$\int_{\xi_0}^{\infty} \left\{\frac{1}{2}(\cosh 2\xi) g_n - \frac{1}{4}[\mathrm{sgn}(n-2) g_{|n-2|} + g_{n+2}]\right\} \times e^{-n\xi}\, d\xi = \delta_{n1}\cos\lambda, \tag{12b}$$

$$\int_{\xi_0}^{\infty} \left\{\frac{1}{2}(\cosh 2\xi) G_n - \frac{1}{4}[\delta_{n2} G_0 + G_{|n-2|} + G_{n+2}]\right\} \times e^{-n\xi}\, d\xi = -\delta_{n1}\sin\lambda. \tag{12c}$$

The above integral conditions represent an essential part of the method of solution. They are used to predict $G_0(\xi_0, t)$, $g_n(\xi_0, t)$, $G_n(\xi_0, t)$ at every time step. In addition, one can easily prove that the satisfaction of the integral condition (12a) is necessary for ensuring the periodicity of pressure on the tube surface. Such a condition is essential in reaching a sensible solution. The problem of pressure periodicity was pointed out earlier in the paper by Panniker and Lavan [28] who studied the early stage of boundary-layer development on the surface of an elliptic cylinder which started its motion impulsively from rest in a quiescent fluid. However, no solution to the problem was provided.

During the first stage of motion, the uniform stream starts suddenly and the viscous region is initially limited to a very thin layer on the tube surface. Following the work by Badr and Dennis [29] and by Badr *et al.* [30], we use the boundary-layer coordinates (z, τ) defined as:

$$\xi = \xi_0 + kz \quad \text{where} \quad k = 2\sqrt{\frac{2\tau}{Re}}, \quad \tau = t.$$

We also introduce ψ^* and ζ^* defined as:

$$\zeta^* = k\zeta \quad \text{and} \quad \psi^* = \frac{\psi}{k}.$$

The above transformation is essential for obtaining accurate results at small times (for details see ref. [29]). After transforming all equations and boundary conditions to the new coordinate system, the numerical solution is carried out closely following the same procedure used in refs. [29, 30] except for the additional coupling resulting from the terms

$$\frac{\partial G_2}{\partial \tau}, \quad \frac{\partial g_{n+2}}{\partial \tau}, \quad \frac{\partial G_{n+2}}{\partial \tau}$$

in equations (8a)–(8c) and also the terms

$$\frac{\partial H_2}{\partial \tau}, \quad \frac{\partial h_{n+2}}{\partial \tau}, \quad \frac{\partial H_{n+2}}{\partial \tau}$$

in equations (10a)–(10c). To overcome this problem, these terms were first approximated and then corrected through an iterative type solution. It is important to mention that the boundary-layer coordinate z will continuously stretch with time when viewed in the physical coordinates. Such behavior matches closely the growth of the boundary-layer region and accordingly assists in obtaining a highly accurate solution.

Staniforth [31] obtained an analytical solution for the governing equations [equations (4)–(5)] in the absence of buoyancy forces ($Gr = 0$) that is applicable at the start of the fluid motion ($t = 0$). Staniforth's solution is used as an initial condition in order to start the numerical scheme. The expressions for ψ^* and ζ^* at $t = 0$ are given by:

$$\psi^* = e^{\xi_0} \sin(\eta - \lambda) \times \left[z \operatorname{erf}(H_{\xi_0}^{1/2} z) + \frac{1}{\pi^{1/2} H_{\xi_0}^{1/2}} (e^{-H_{\xi_0} z^2} - 1) \right], \quad (13a)$$

$$\zeta^* = \frac{2e^{\xi_0}}{\pi^{1/2} H_{\xi_0}^{1/2}} \sin(\eta - \lambda)\, e^{-H_{\xi_0} z^2}, \quad (13b)$$

where $H_{\xi_0} = \frac{1}{2}(\cosh 2\xi_0 - \cos 2\eta)$.

In order to express the surface pressure variation and the local Nusselt number distribution in terms of the dimensionless variables used in this study, let us first introduce the dimensionless pressure p^* defined as:

$$p^* = \frac{p - p_\pi}{\frac{1}{2}\rho u_\infty^2}.$$

One can apply the Navier–Stokes equations at the cylinder surface to obtain:

$$\left(\frac{\partial p^*}{\partial \eta}\right)_{\xi_0} = -\frac{4}{Re}\left(\frac{\partial \zeta}{\partial \xi}\right)_{\xi_0}.$$

By integrating the above expression w.r.t. η on the surface $\xi = \xi_0$, we obtain:

$$p^* = -\frac{4}{Re}\left[\frac{1}{2}\frac{\partial G_0}{\partial \xi}(\eta - \pi) + \sum_{n=1}^{N} \frac{1}{n} \times \left\{ \frac{\partial G_n}{\partial \xi} \sin n\eta - \frac{\partial g_n}{\partial \xi}(\cos n\eta - \cos n\pi) \right\}\right]. \quad (14)$$

The periodicity of p^* requires that $(\partial G_0/\partial \xi)_{\xi_0}$ must be zero at all times. This is implicitly satisfied by the integral conditions given in equation (12a).

The local heat transfer coefficient h is defined as:

$$h = \frac{-k}{T_s - T_\infty}\left(\frac{\partial T}{\partial r}\right)_{\xi_0},$$

where k is the fluid conductivity and r is a linear coordinate normal to the tube surface. In terms of the elliptic coordinate ξ, the above expression can be written as:

$$h = -\frac{k/c}{H_{\xi_0}^{1/2}}\left(\frac{\partial \phi}{\partial \xi}\right)_{\xi_0}.$$

We now define the local Nusselt number Nu as:

$$Nu = \frac{2ah}{k} = -\frac{2\cosh \xi_0}{H_{\xi_0}^{1/2}}\left(\frac{\partial \phi}{\partial \xi}\right)_{\xi_0}, \quad (15)$$

and the average Nusselt number $\overline{Nu}$ can be obtained from:

$$\overline{Nu} = \frac{1}{L}\int_0^L Nu\, ds,$$

where L is the elliptic section perimeter and ds is an elementary length along that perimeter. The final expression for $\overline{Nu}$ is:

$$\overline{Nu} = -\frac{2\pi}{(L/a)}\left(\frac{\partial H_0}{\partial \xi}\right)_{\xi_0}. \quad (16)$$

4. DISCUSSION OF RESULTS

Before presenting results we will first discuss the accuracy of the method of solution and the numerical scheme used during the two stages of flow development. The test case for the first stage is to study the early stage of flow development over an elliptic cylinder started its motion impulsively from rest in a quiescent fluid. The cylinder has an axis ratio $A_r = 0.6$ and inclined at an angle $\lambda = 30°$ while the flow Reynolds number is 5000. This problem was solved analytically by Staniforth [31] who obtained a series solution (in boundary-layer coordinates) that is only valid for small times. Figure 2 shows a comparison between the surface vorticity distribution obtained using the present method and Staniforth's analytical solution. The test case for the second stage is to study the forced convection from an elliptic cylinder of axis ratio close to unity ($A_r = 0.96$) and compare with available data for the case of a circular cylinder. Table 1 shows a comparison between the present results and those obtained by Hatton *et al.* [32], Collis and Williams

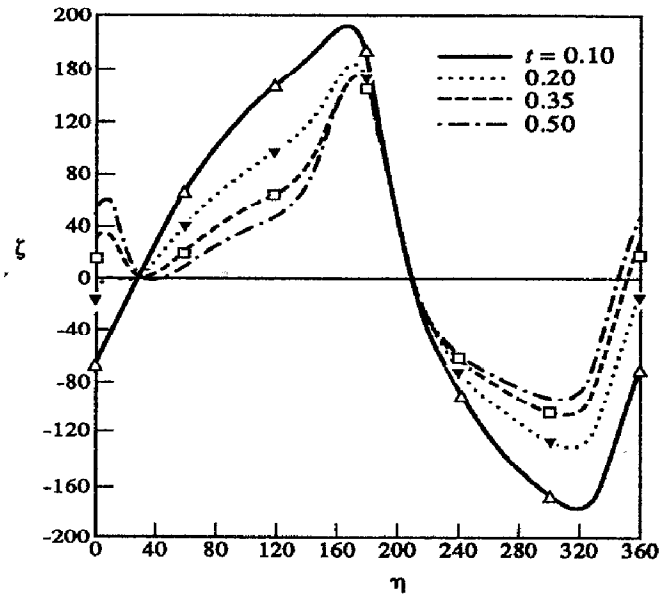

FIG. 2. Comparison between the obtained surface vorticity distribution and Staniforth's analytical solution [31] for the case of $Re = 5000$, $A_r = 0.6$, and $\lambda = 30°$. Present study: (———) $t = 0.1$; (· · · · ·) $t = 0.2$; (— — —) $t = 0.35$; (— · — · —) $t = 0.5$. Staniforth's solution: △—$t = 0.1$; ▽—$t = 0.2$; □—$t = 0.35$.

Table 2. The effect of Grashof number on the average Nusselt number ($A_r = 0.6$ and $\lambda = 30°$)

Re	Gr/Re^2	$\overline{Nu}$	$\overline{Nu}/\overline{Nu_f}$
20	0.00	2.911	1.000
	1.95	3.028	1.040
	3.90	3.247	1.115
	5.86	3.445	1.183
	9.76	3.757	1.291
50	0.00	4.364	1.000
	1.95	4.581	1.050
	3.90	4.919	1.127
	5.86	5.204	1.193
	9.76	5.649	1.295
100	0.00	6.030	1.000
	1.95	6.380	1.058
	3.90	6.780	1.124
	5.86	7.120	1.181
	9.76	7.700	1.277
200	0.00	8.890	1.000
	1.00	9.283	1.044
	2.00	9.401	1.057
	3.00	9.573	1.077
	5.00	10.055	1.131
500	0.00	15.600	1.000
	1.00	16.230	1.040
	2.00	16.680	1.069
	3.00	16.800	1.077
	5.00	17.820	1.142

[33], and Dennis *et al.* [34]. The table shows a maximum difference of 7.2% with ref. [32], 8.7% with ref. [33], and 2.3% with ref. [34]. Part of these differences are attributed to the difference in the cylinder geometry.

The effect of Grashof number on the average Nusselt number is investigated for a cylinder of axis ratio $A_r = 0.6$ inclined at an angle $\lambda = 30°$. The investigation covered Reynolds numbers ranging from 20 to 500 and Grashof numbers ranging from 0 to 1.25×10^6. Table 2 shows the steady or the time average of the quasi-steady values of $\overline{Nu}$ and $\overline{Nu}/\overline{Nu_f}$ for every considered value of Gr (or Gr/Re^2), where $\overline{Nu_f}$ is the average Nusselt number for the forced convection regime ($Gr = 0$). The table shows the clear dependence of $\overline{Nu}/\overline{Nu_f}$ on the term Gr/Re^2 with negligible dependence on Re. The term Gr/Re^2 represents the ratio between buoyancy and inertia forces. An increase of Gr/Re^2 from 0 to 5 causes about a 14% increase of $\overline{Nu}/\overline{Nu_f}$ in the entire range of Re considered. The graphical representation of the relation between $\overline{Nu}/\overline{Nu_f}$ and Gr/Re^2 can be seen in Fig. 3.

The effect of increasing Gr on the local Nusselt number and surface vorticity distributions is shown in Fig. 4a and b for the case of $\lambda = 30°$ and $Re = 20$. Figure 4a shows a maximum local Nusselt number at $\eta = 180°$ and a minimum at η between 60° and 100°. Moreover, the increase of Gr causes Nu to increase on the entire surface except for the region $60° < \eta < 135°$ at which the effect is reversed. To understand this phenomenon, the surface vorticity distribution plotted in Fig. 4b shows that the absolute value of ζ increases with the increase of Gr over most of the tube surface, indicating a higher velocity gradient which is expected as a result of the increase in buoyancy forces. Such a velocity increase near the tube surface leads to an increase in the heat transfer rate. Figure 5a and b shows the local Nusselt number and vorticity variations for the case of $Re = 200$. The region $0 < \eta < 100°$ is characterized by vortex formation and shedding and the effect of such velocity field on Nu and ζ can be seen in this figure. As a result, the flow and thermal fields continue to fluctuate and accordingly the Nu and ζ distributions given in Fig. 5a and

Table 1. Comparison between the obtained average Nusselt numbers for $A_r = 0.96$ and the results reported by Hatton *et al.* [32], Collis and Williams [33], and Dennis *et al.* [34] for the case of forced convection from a circular cylinder

Re	$\overline{Nu}$ ($A_r = 0.96$) present study	Ref. [32]	$\overline{Nu}$ ($A_r = 1.0$) Ref. [33]	Ref. [34]
5	1.456	1.561	1.395	1.423
20	2.550	2.548	2.396	2.557
40	3.490	3.318	3.185	3.480

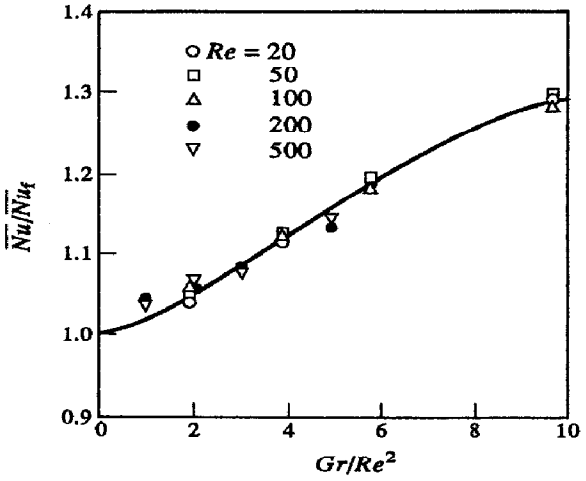

FIG. 3. The effect of increasing Gr/Re^2 on the ratio $\overline{Nu}/\overline{Nu_f}$ for the case of $A_r = 0.6$ and $\lambda = 30°$.

b are continuously changing with time. The figures represent the situation at $t = 20$.

The effect of Gr on the streamline and isotherm patterns for the case of $Re = 20$ is shown in Figs. 6 and 7 for $Gr/Re^2 = 0$ and 1.95 and in Figs. 8 and 9 for the case of $Re = 200$ and $Gr/Re^2 = 0$ and 5. In the first case ($Re = 20$), both velocity and thermal fields reached steady state with no vortex shedding. Figure 6a and b shows that the increase of Gr not only moves the rear stagnation point but also removes the separation bubble behind the tube section. The effect of buoyancy forces on the shape of isotherm contours downstream of the tube is clearly shown in Fig. 7a and b. Figure 8a and b shows that vortex formation and shedding take place in the case of $Re = 200$. However, it is clear that vortex formation is greatly suppressed as Gr increases. The effect of vortex shedding on the thermal field is shown in Fig. 9a where a lump of warm fluid is separated and convected downstream. Since the flow and thermal fields in this case ($Re = 200$) are continuously changing with time, the plotted streamline and isotherm patterns show only the situation at $t = 20$.

The effect of the inclination angle λ on the rate of heat transfer is only studied for the cases of $Re = 20$ and 200 when $A_r = 0.6$ and $Gr/Re^2 = 2$. The values of λ considered vary between 0° and 150° with a step of 30°. The case of $\lambda = 180°$ was excluded since it is exactly the same as $\lambda = 0$. The numerical values of $\overline{Nu}$ for everyone of the above cases are given in Table 3.

These represent the final steady values for the case of $Re = 20$ and the time average for the case of $Re = 200$ because of the thermal field unsteadiness in the later. The table shows maximum heat transfer rate at $\lambda = 0°$ in the case of $Re = 20$ and at $\lambda = 60°$ in the case of $Re = 200$. The minimum value of $\overline{Nu}$ occurs at $\lambda = 90°$ in the case of $Re = 20$ and at $\lambda = 150°$ in the case of $Re = 200$. However, the maximum percentage change of $\overline{Nu}$ due to changing the angle of inclination did not exceed 6.7% for the two cases considered.

The time variation of $\overline{Nu}$ following the sudden temperature increase is shown in Fig. 10a for the case of $Re = 20$ and in Fig. 10b for the case of $Re = 200$. The angles of inclination considered are 0°, 30°, 90°, and 150° in each case. Although $\overline{Nu}$ reached its final steady value in the first case ($Re = 20$), it continued to fluctuate in the second ($Re = 200$) because of vortex shedding. Moreover, the amplitude of oscillation of $\overline{Nu}$ depends on λ as can be seen in Fig. 10b. As λ approaches 90° the amplitude gets larger and vice versa. The effect of λ on the local Nusselt number distribution is shown in Fig. 11a for the case of $Re = 20$ and in Fig. 11b for the case of $Re = 200$. Although the values of $\overline{Nu}$ did not change much with the change in λ, the local Nu distribution is greatly affected because of the considerable change in the velocity field. One should mention here that Fig. 11a represents a steady thermal field while Fig. 11b represents a quasi-steady field due to vortex shedding.

The effect of λ on the streamline and isotherm patterns is shown in Figs. 12 and 13 for the case of $Re = 200$ and $Gr = 8 \times 10^4$ when λ varies between 0° and 150°. Figure 12 shows the clear dependence of the size of the shedding vortices on the angle of inclination λ. As λ approaches 90° bigger vortices are formed and vice versa. This explains the higher fluctuations in the average Nusselt number when $\lambda = 90°$ that was pointed out earlier in Fig. 11b.

5. CONCLUSIONS

The problem of mixed convection from a straight isothermal elliptic tube is solved numerically in the Reynolds number range of 20–500 for Grashof numbers ranging from 0 to 1.25×10^6 and for angles of inclination ranging from 0° to 180°. The solution is based on a numerical integration of the conservation equations of mass, momentum, and energy with no boundary-layer approximations. The obtained velocity and thermal fields are found to be either steady or quasi-steady depending on Reynolds and Grashof numbers. Vortex shedding causes unsteadiness in both flow and thermal fields. It is found that the increase of Gr for a given value of Re results in suppressing vortex formation and shedding. The average Nusselt number is found to increase considerably with the increase of the ratio Gr/Re^2. The effect of the inclination angle on the rate of heat transfer is found not to exceed 6.7% for the range of variables considered. However, the fluctuations in the average Nusselt number increase as λ approaches 90°. The details of the velocity and thermal fields are presented in the form of isotherm and streamline patterns in addition to the surface vorticity and local Nusselt number distributions. It is hoped that this work represents a step forward towards the solution of the more difficult problem of forced (or mixed) convection from an inclined finite flat plate.

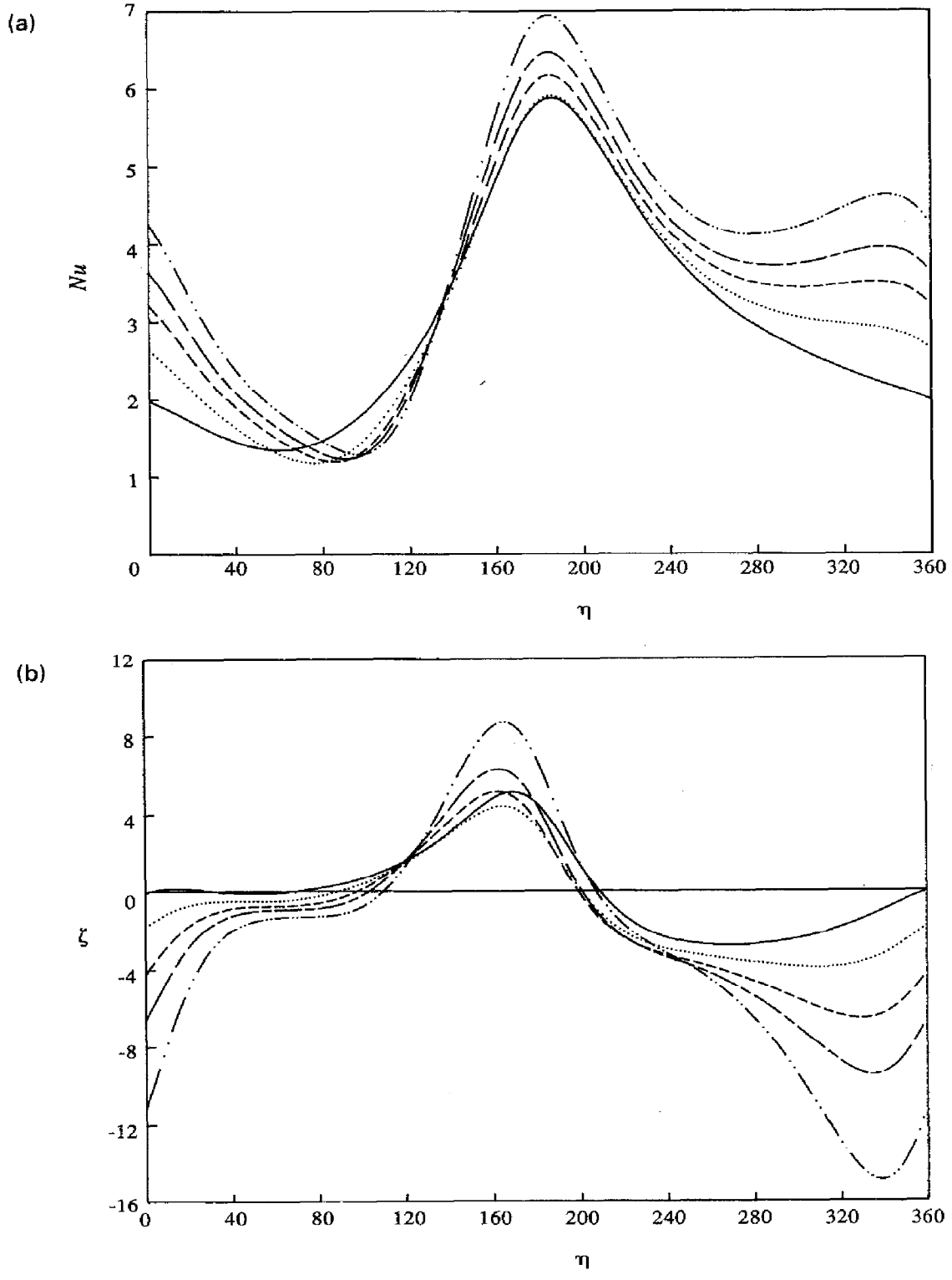

FIG. 4. The effect of increasing Grashof number on the local Nusselt number and surface vorticity distributions for the case of $Re = 20$ and $\lambda = 30°$: (a) local Nusselt number; (b) surface vorticity: (———)—$Gr/Re^2 = 0$; (· · · ·)—$Gr/Re^2 = 1.95$; (– – – –)—$Gr/Re^2 = 3.90$; (— — — —)—$Gr/Re^2 = 5.86$; (– · – · –)—$Gr/Re^2 = 9.76$.

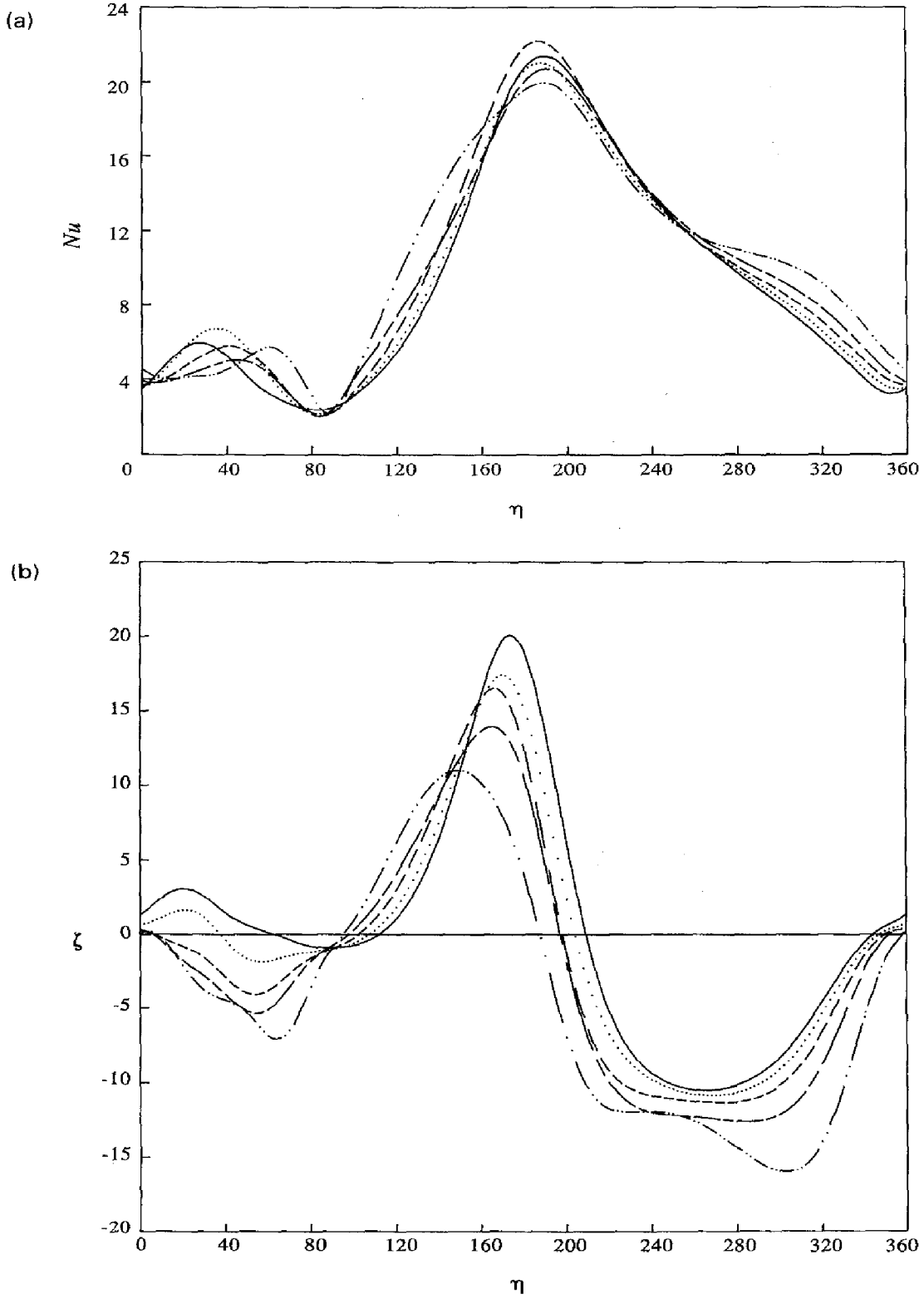

FIG. 5. The effect of increasing Grashof number on the local Nusselt number and surface vorticity distributions for the case of $Re = 200$, and $\lambda = 30°$: (a) local Nusselt number; (b) surface vorticity: (———)—$Gr/Re^2 = 0$; (· · · ·)—$Gr/Re^2 = 1.0$; (– – – –)—$Gr/Re^2 = 2.0$; (——— · ———)—$Gr/Re^2 = 3.0$; (– · – · – · –)—$Gr/Re^2 = 5.0$.

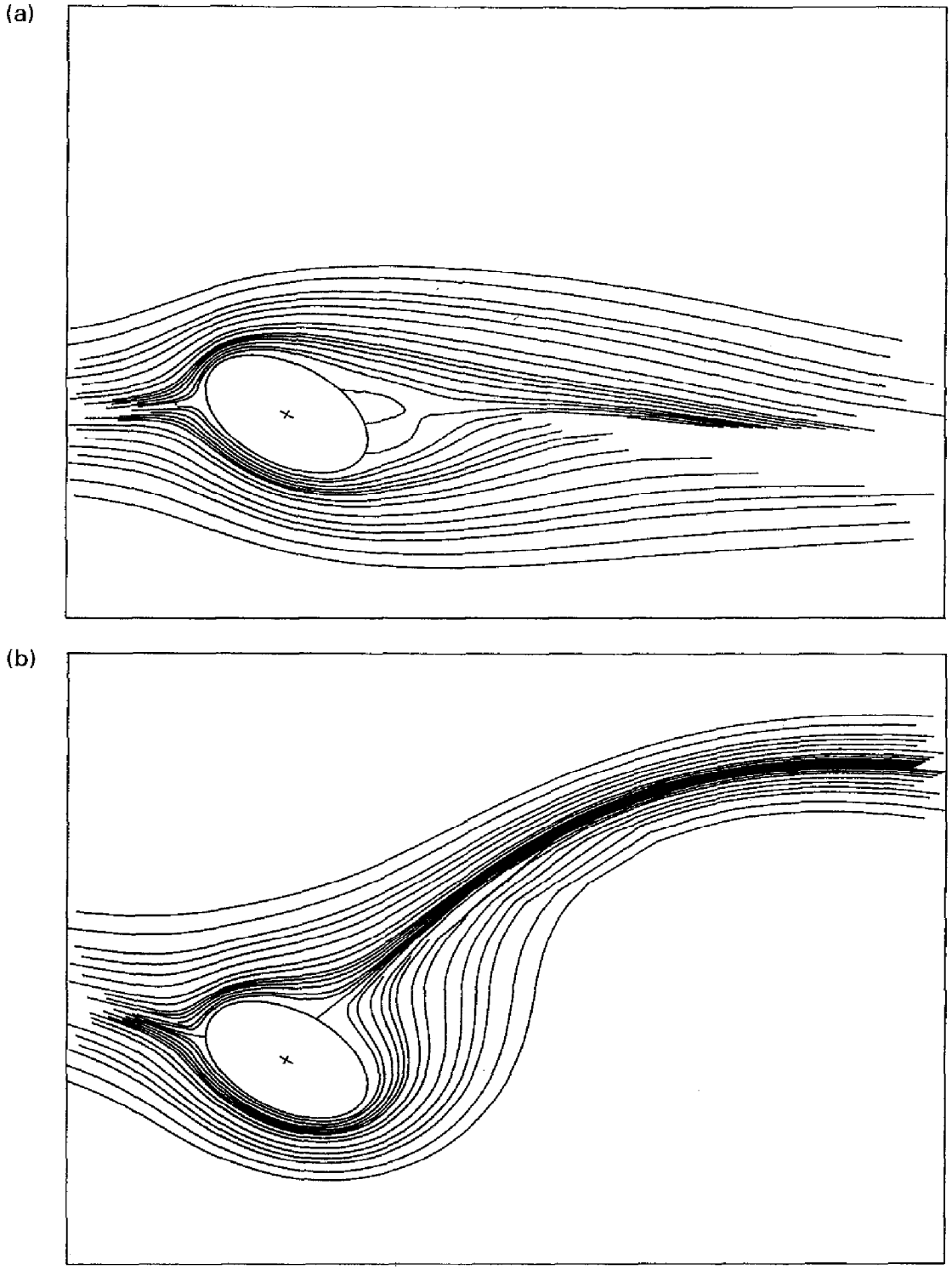

FIG. 6. The streamline patterns for the case of $Re = 20$ and $\lambda = 30°$: (a) $Gr/Re^2 = 0$, (b) $Gr/Re^2 = 1.95$. Streamlines plotted are $\psi = -1.0, -0.8, -0.6(0.1), -0.2, -0.15, -0.1, -0.08\ (0.02), -0.02, -0.01\ (0.01), 0.02, 0.04\ (0.02), 0.1, 0.15, 0.2\ (0.1), 0.6, 0.8, 1.0$.

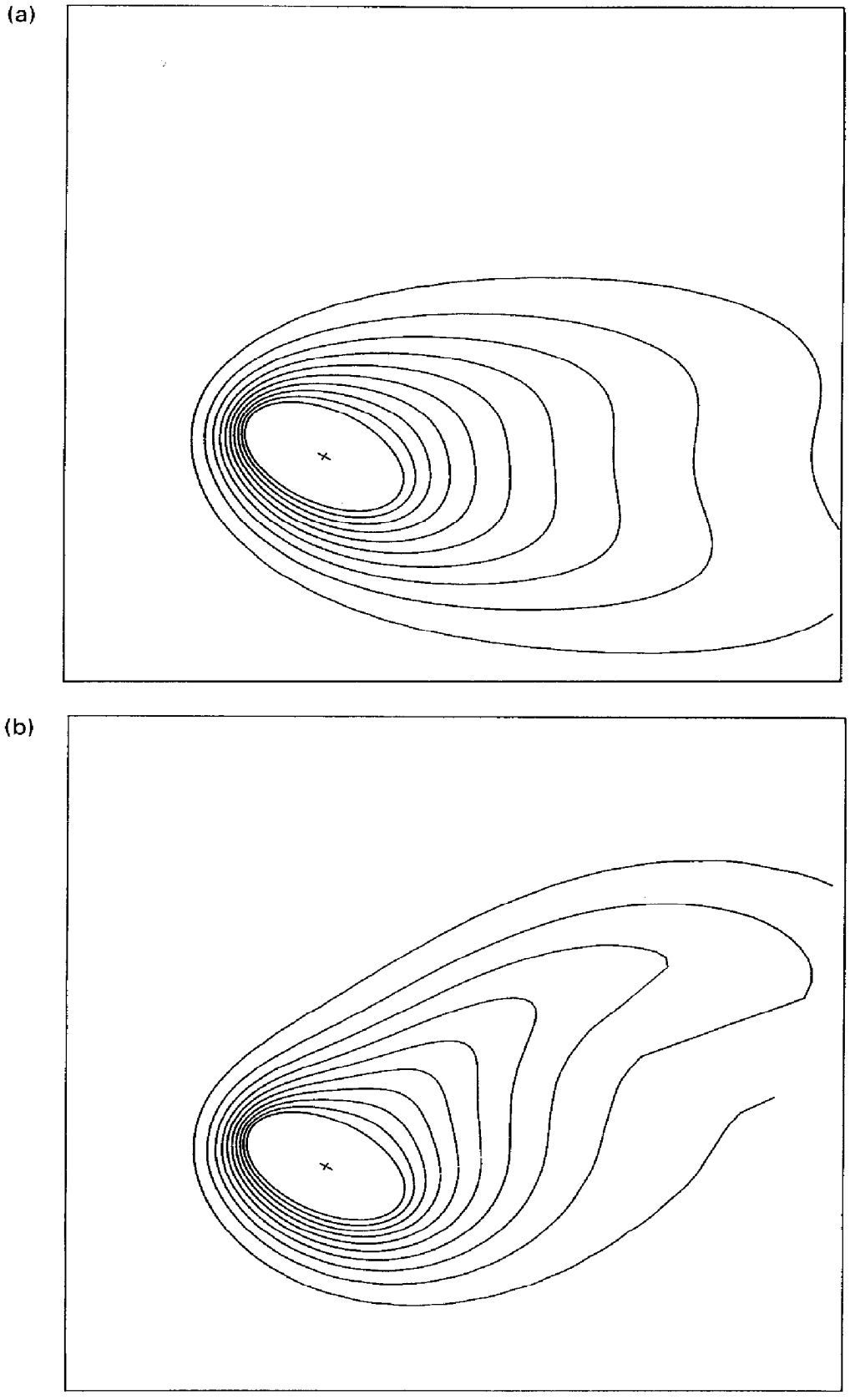

FIG. 7. The isotherm contours for the case of $Re = 20$ and $\lambda = 30°$: (a) $Gr/Re^2 = 0$; (b) $Gr/Re^2 = 1.95$. Isotherms plotted are $\phi = 0.1, 0.2, \ldots, 0.9$.

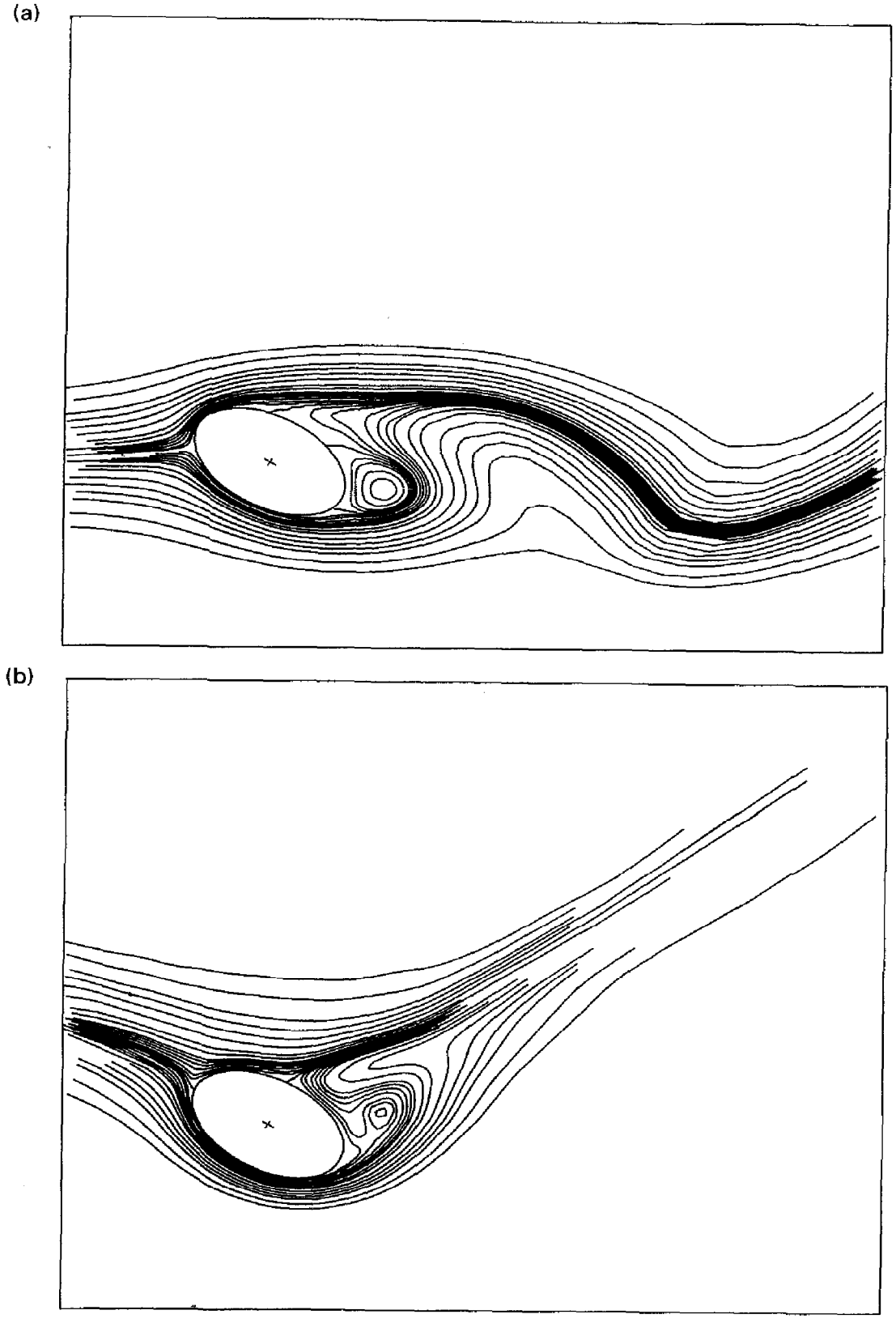

FIG. 8. The streamline patterns for the case of $Re = 200$ and $\lambda = 30°$ at time $t = 20$: (a) $Gr/Re^2 = 0$; (b) $Gr/Re^2 = 5.0$. Streamlines plotted are the same as in Fig. 6.

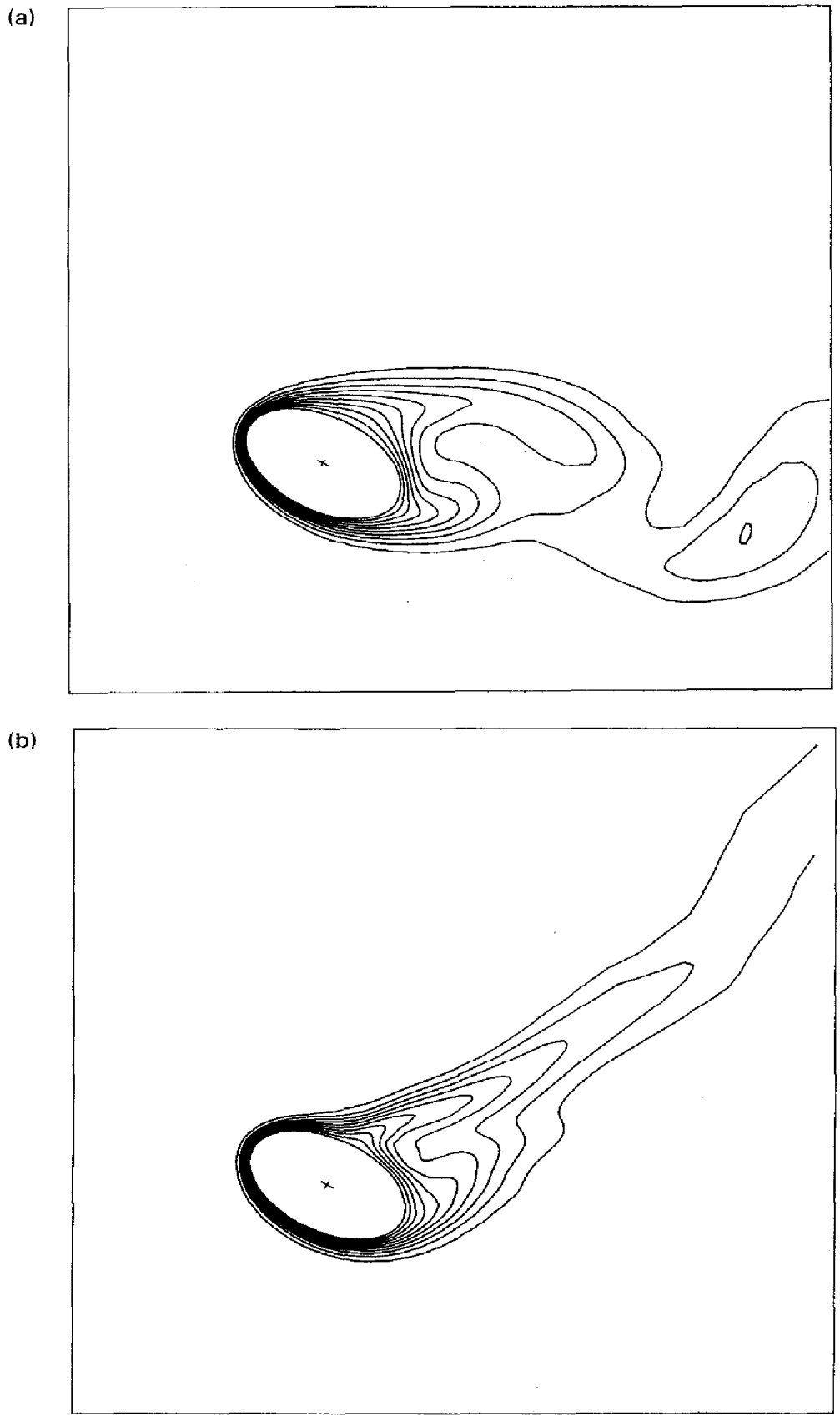

FIG. 9. The isotherm contours for the case of $Re = 200$ and $\lambda = 30°$ at time $t = 20$: (a) $Gr/Re^2 = 0$ (b) $Gr/Re^2 = 5.0$. Isotherms plotted are the same as in Fig. 7.

Table 3. The effect of the inclination angle on the average Nusselt number for the two cases of $Re = 20$ and $Re = 200$ ($A_r = 0.6$ and $Gr/Re^2 = 2.0$)

Re	λ	$\overline{Nu}$
20	0°	3.14
	30°	3.06
	60°	2.96
	90°	2.93
	120°	2.96
	150°	2.99
200	0°	9.32
	30°	9.21
	60°	9.53
	90°	9.51
	120°	9.03
	150°	8.89

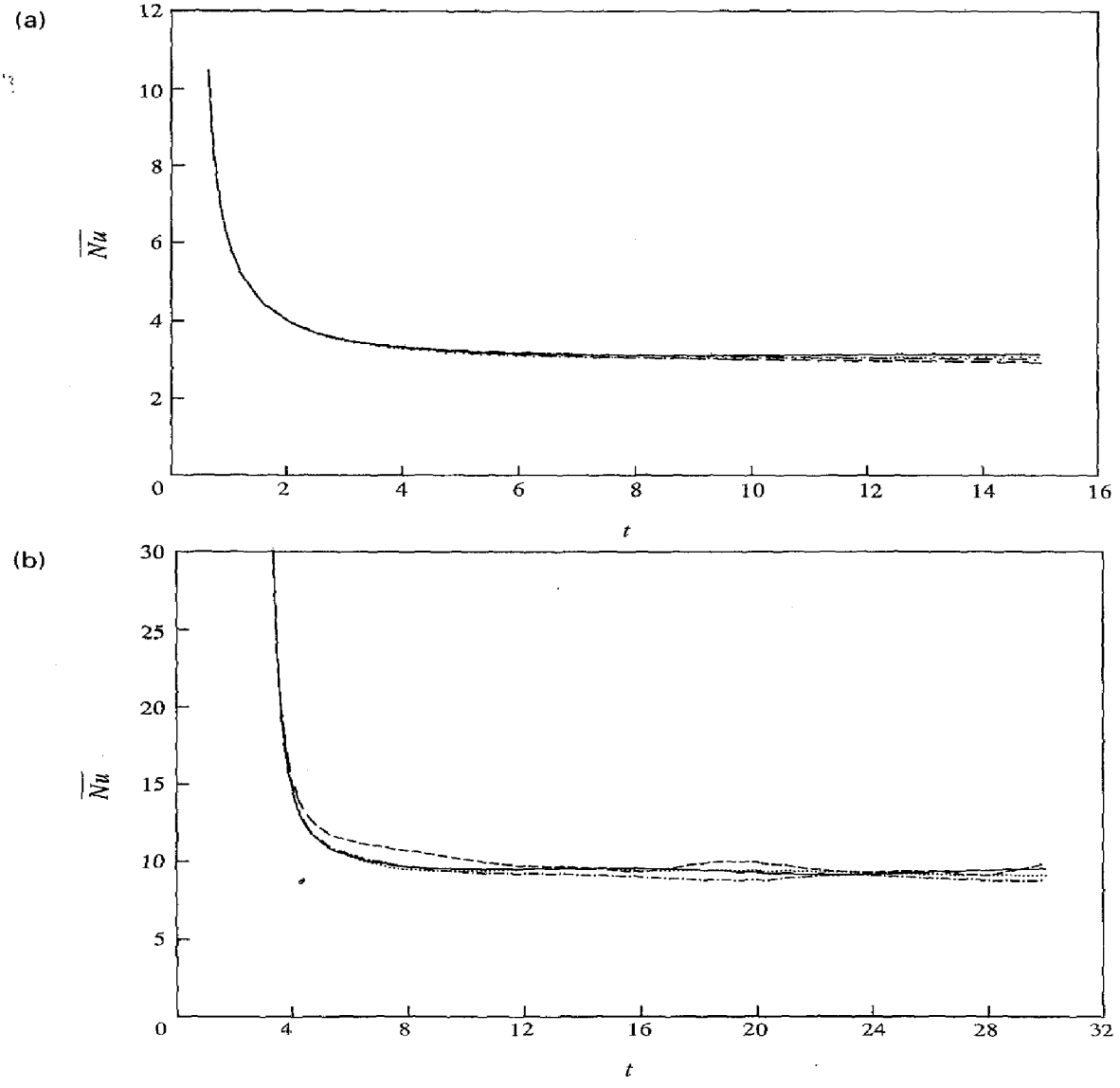

FIG. 10. The time variation of $\bar{N}_u$ following the sudden temperature rise for various inclination angles λ: (a) $Re = 20$ and $Gr/Re^2 = 3.9$; (b) $Re = 200$ and $Gr/Re^2 = 2.0$: (———)—$\lambda = 0°$; (· · · ·)—$\lambda = 30°$; (– – – –)—$\lambda = 90°$; (– · – · –)—$\lambda = 150°$.

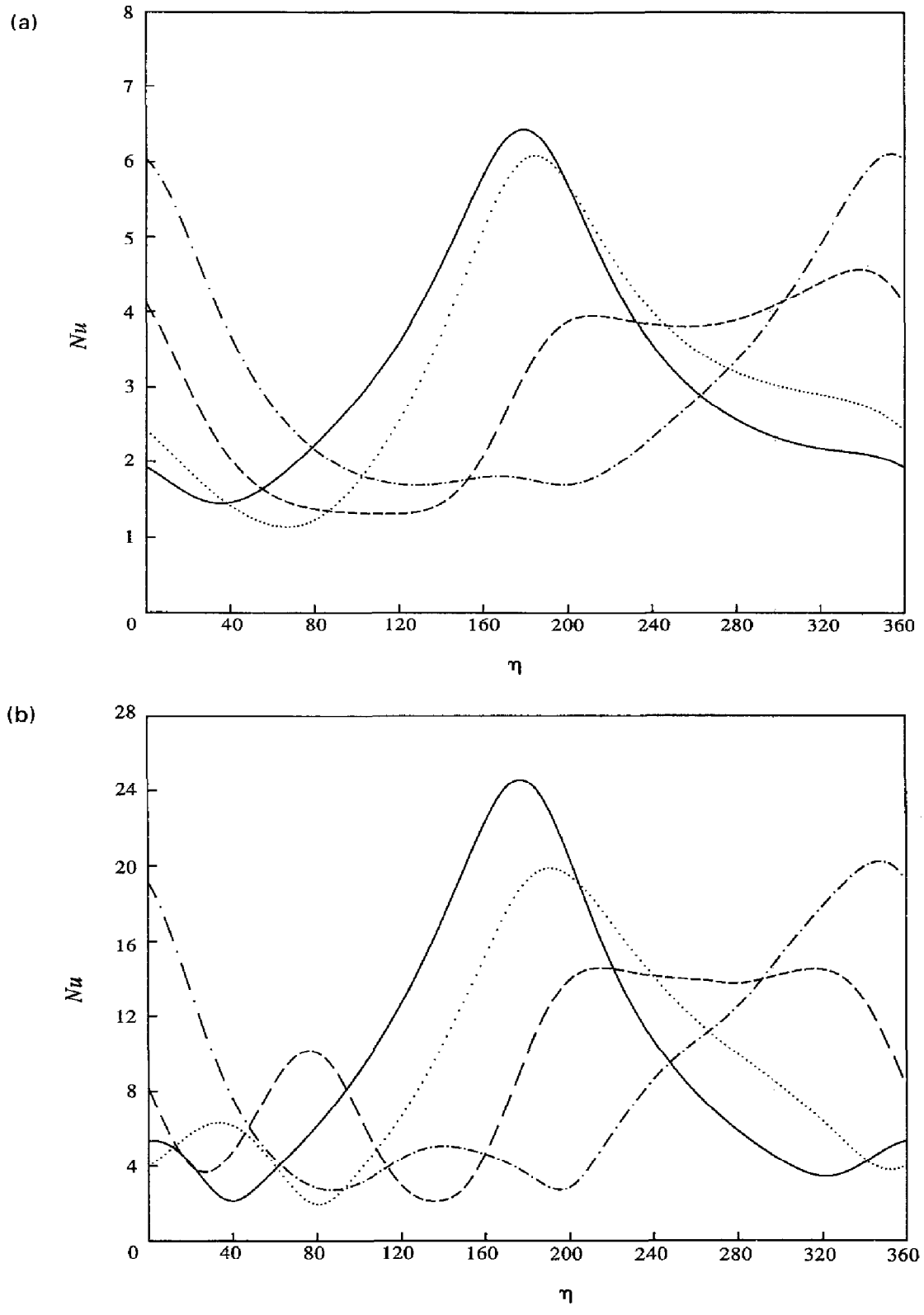

FIG. 11. The effect of the inclination angle λ on the local Nusselt number distribution: (a) $Re = 20$ and $Gr/Re^2 = 3.9$ at $t = 15$; (b) $Re = 200$ and $Gr/Re^2 = 2.0$ at $t = 30$: (———)—$\lambda = 0°$; (· · · ·)—$\lambda = 30°$; (– – –) $\lambda = 90°$; (– · – · –)—$\lambda = 150°$.

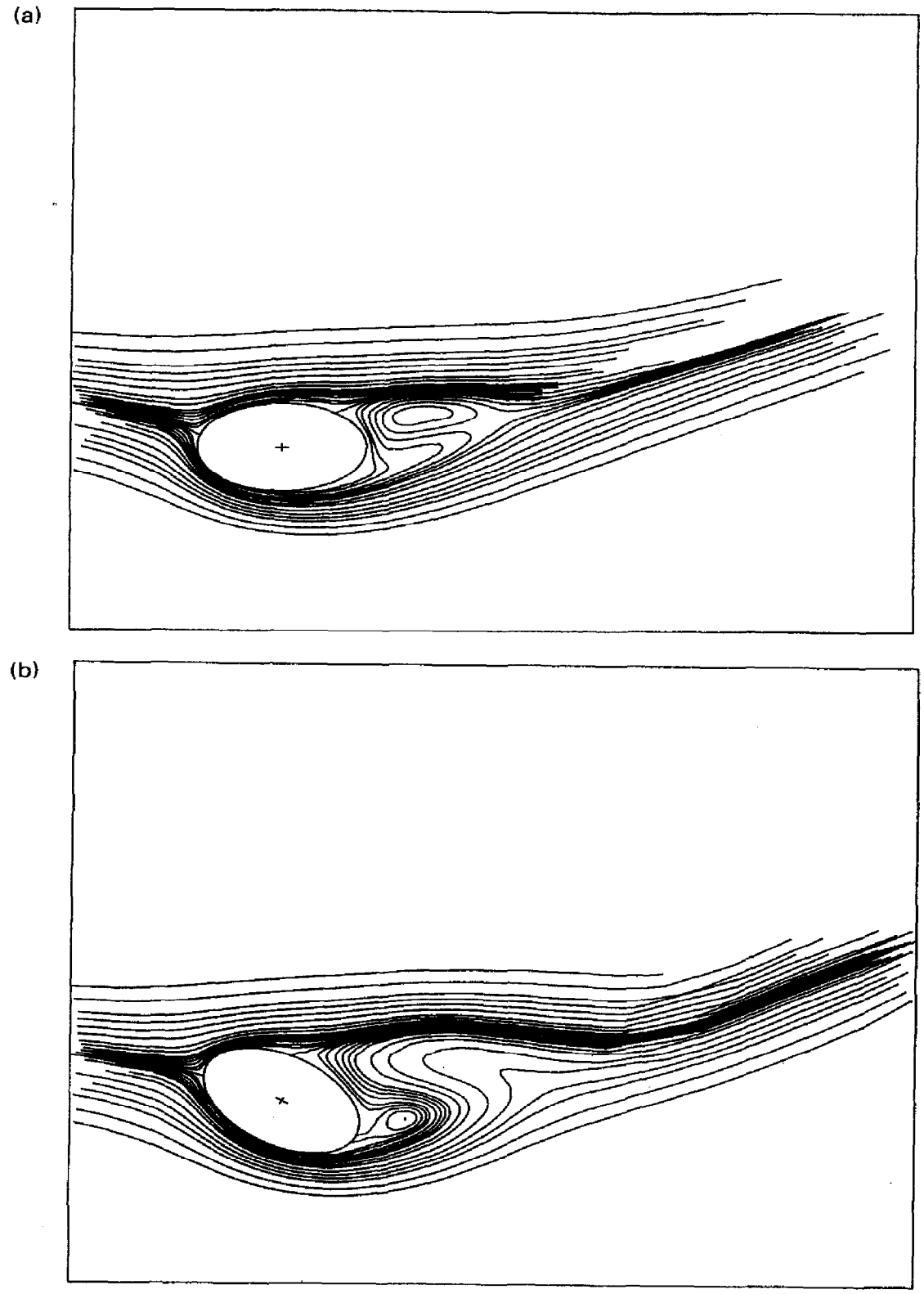

FIG. 12. The effect of the inclination angle λ on the streamline pattern for the case of $Re = 200$ and $Gr/Re^2 = 2.0$: (a) $\lambda = 0°$; (b) $\lambda = 30°$; (c) $\lambda = 60°$; (d) $\lambda = 90°$; (e) $\lambda = 120°$; and (f) $\lambda = 150°$. Streamlines plotted are the same as in Fig. 6.

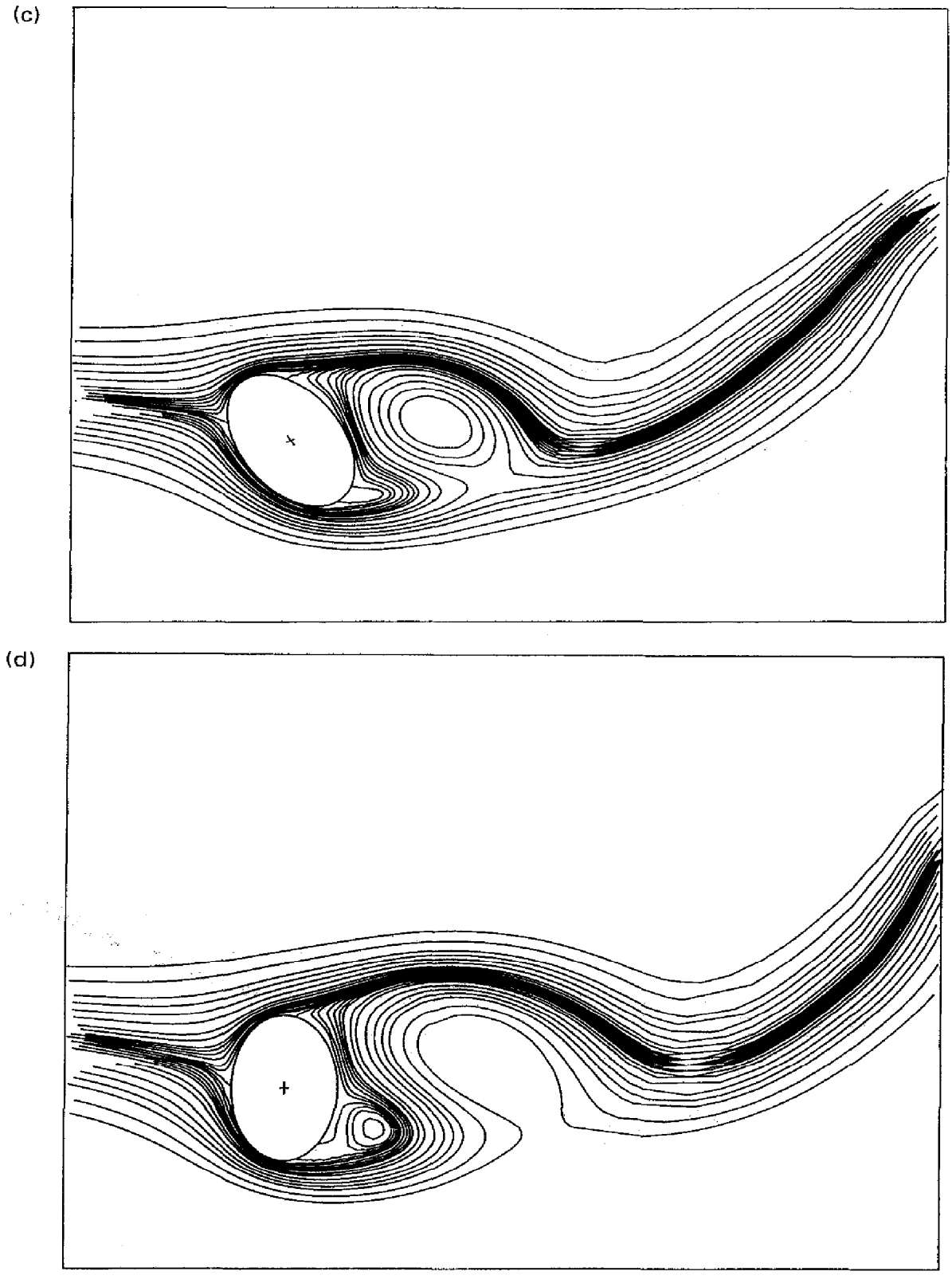

FIG. 12—*continued.*

(e)

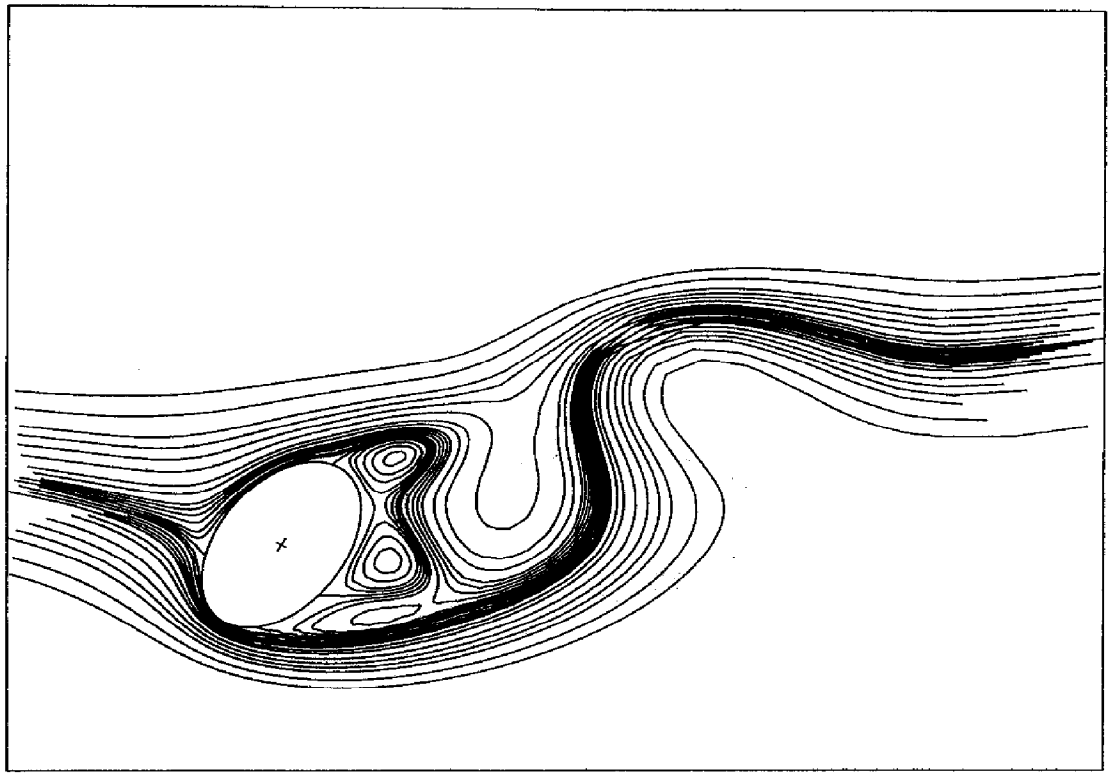

(f)

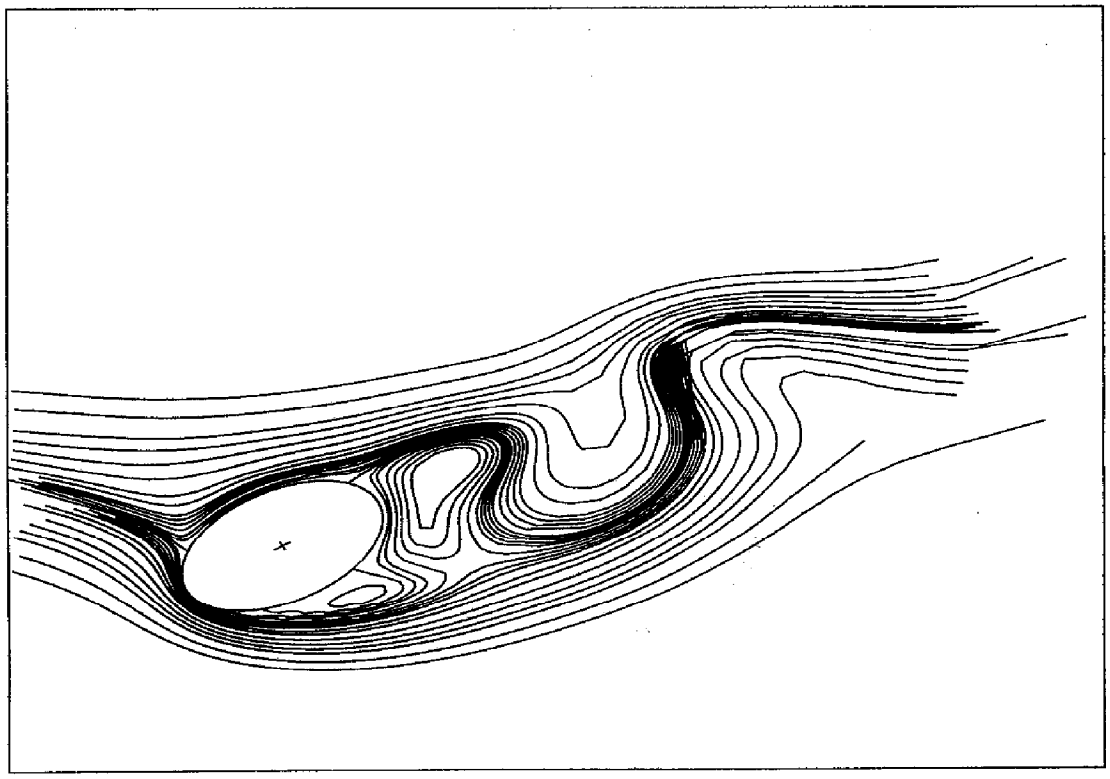

FIG. 12—*continued.*

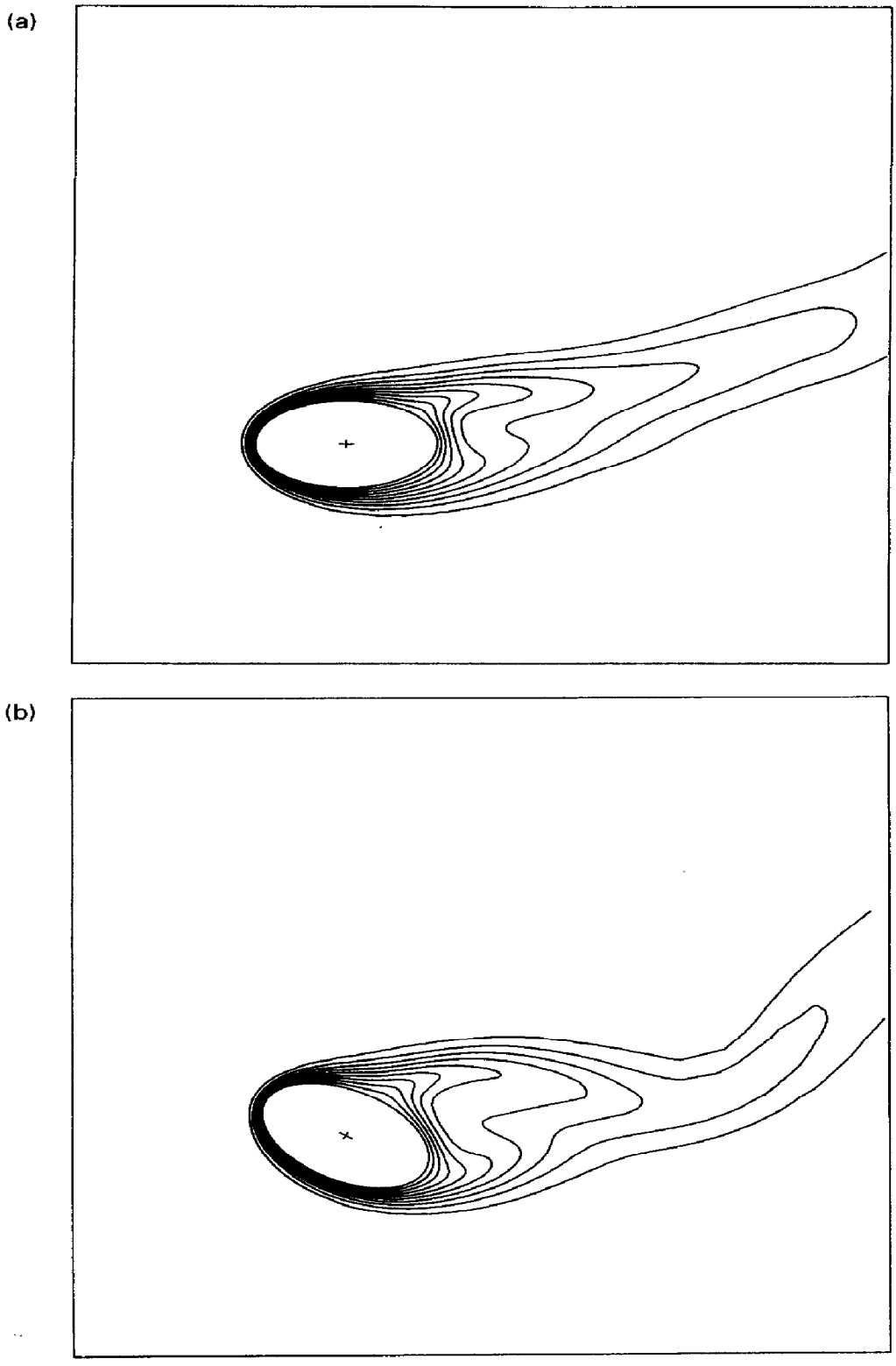

FIG. 13. The effect of the inclination angle λ on the isotherm contours for the case of $Re = 200$ and $Gr/Re^2 = 2.0$: (a) $\lambda = 0°$; (b) $\lambda = 30°$; (c) $\lambda = 60°$; (d) $\lambda = 90°$; (e) $\lambda = 120°$; and (f) $\lambda = 150°$. Isotherms plotted are the same as in Fig. 7.

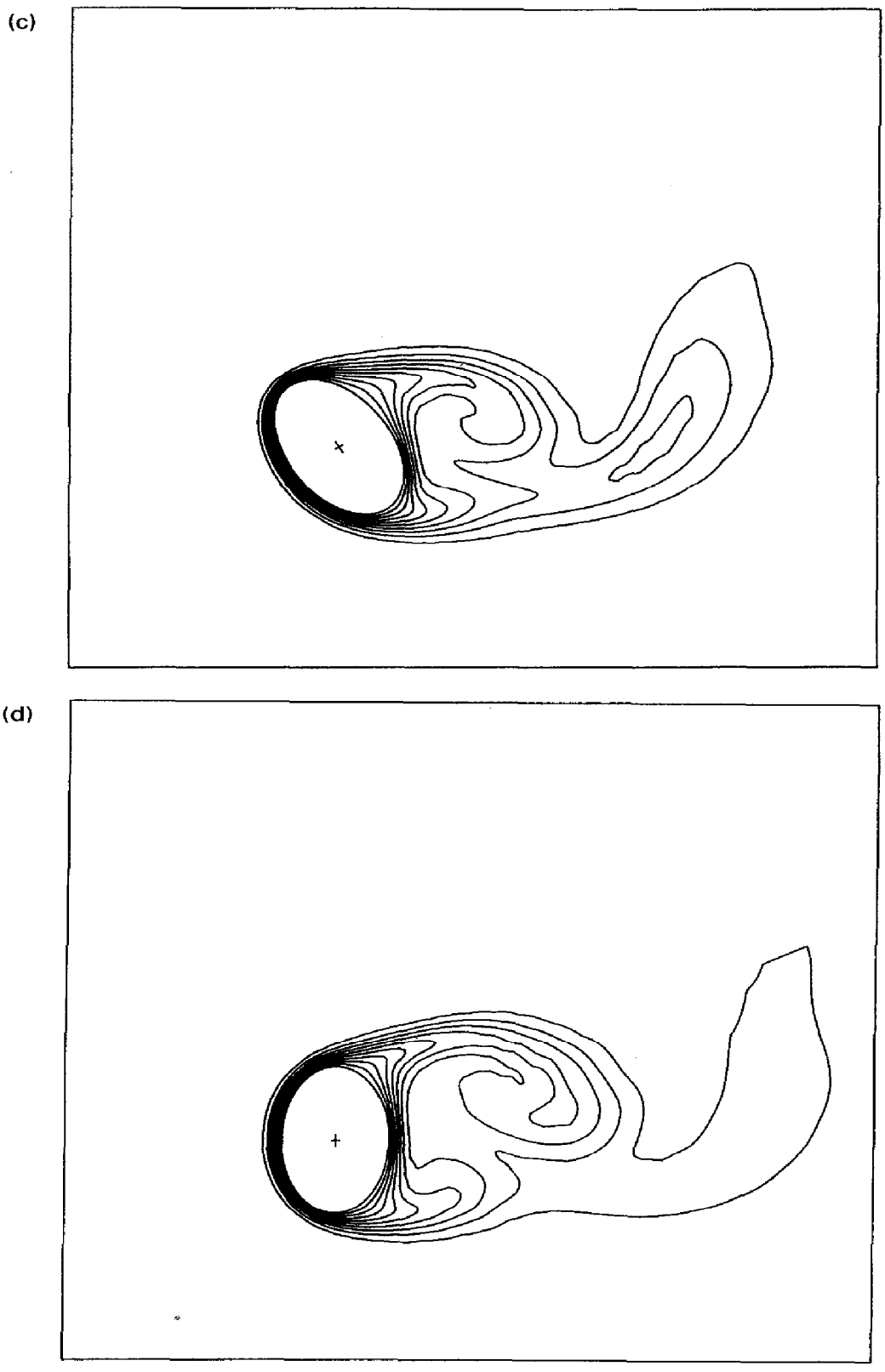

FIG. 13—*continued.*

(e)

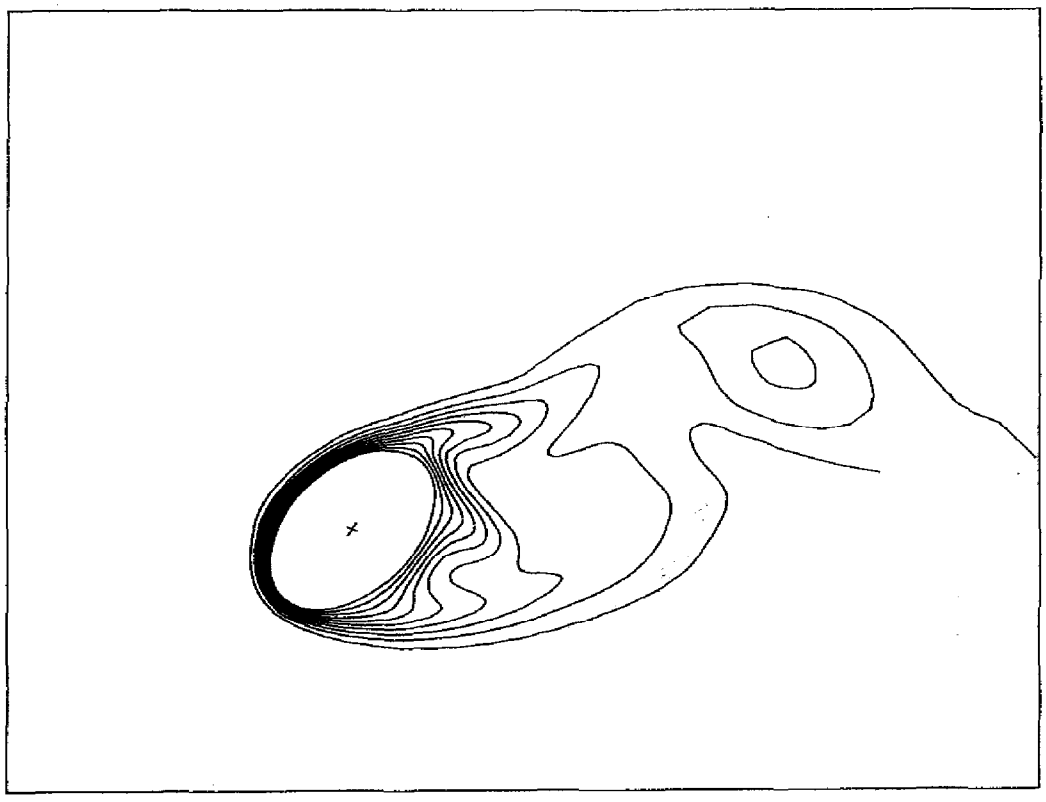

(f)

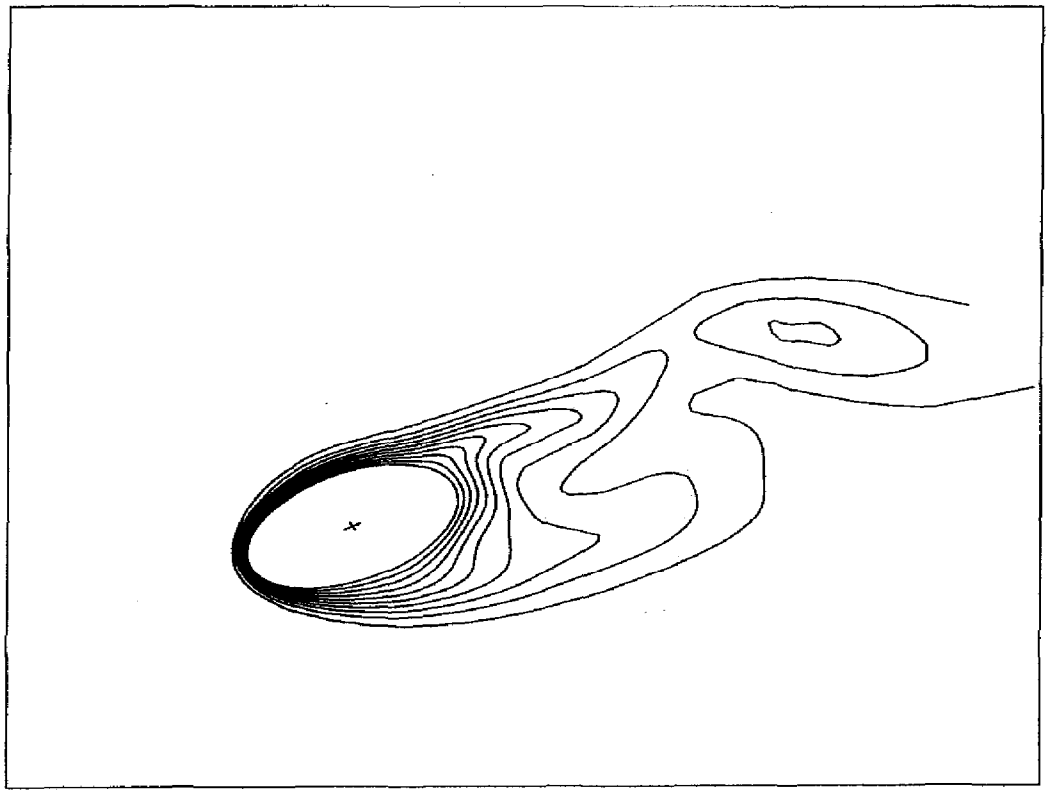

FIG. 13—*continued.*

Acknowledgements—This work was carried out during sabbatical leave at the University of Western Ontario (UWO), London, Canada. The author wishes to acknowledge the support received from King Fahd University of Petroleum and Minerals and also the nice work environment provided by UWO during the course of this study.

REFERENCES

1. H. Hasimoto, On the flow of a viscous fluid past an inclined elliptic cylinder at small Reynolds numbers, *J. Phys. Soc. Japan* **8,** 653–661 (1953).
2. S. Tomotika and T. Aoi, The steady flow of a viscous fluid past an elliptic cylinder and a flat plate at small Reynolds numbers, *Q. J. Mech. Appl. Math.* **6,** 290–312 (1953).
3. I. Imai, A new method for solving Oseen's equations and its application to the flow past an inclined elliptic cylinder, *Proc. R. Soc. London* **A224,** 141–160 (1954).
4. H. Lugt and H. Haussling, Laminar flow past an abruptly accelerated elliptic cylinder at 45° incidence, *J. Fluid Mech.* **65,** 711–734 (1974).
5. S. Dennis, The computation of two-dimensional asymmetrical flows past cylinders, *SIAM–AMS Proceedings* **11,** 156–177. Providence, Rhode Island (1978).
6. K. Shintani, A. Umemura and A. Takano, Low-Reynolds-number flow past an elliptic cylinder, *J. Fluid Mech.* **136,** 277–289 (1983).
7. K. Izumi, K. Kuwahara, K. Horiuti and K. Oshima, Flow past an elliptic cylinder started impulsively, *Proceedings of the Second International Symposium on Flow Visualization*, pp. 343–347. Fed. Rep. Germany (9–12 September 1980).
8. O. Daube, L. Ta Phuoc, M. Coutanceau and P. Monnet, Numerical and experimental study of the unsteady viscous flow generated by an impulsively started elliptic cylinder, *Proceedings of the International Conference on Computational Methods and Experimental Measurements*, pp. 763–773. Southampton, U.K. (1982).
9. T. Tanahashi, T. Sawada, E. Kanai, A. Chino and T. Ando, Unsteady forces on a body immersed in a viscous fluid, *Bull. JSME* **29,** 3717–3724 (1986).
10. N. Nees, Laminar separating flow over nonlifting ellipses, *AIAA. J.* **13,** 688–690 (1975).
11. G. B. Schubauer, Air flow in the boundary layer of an elliptic cylinder, NACA Tech. Rep., No. 652 (1939).
12. N. Delay and N. Sorensen, Low speed drag of cylinders of various shapes, NACA Tech. Note, No. 3038 (1953).
13. V. Modi and E. Wiland, Unsteady aerodynamics of stationary elliptic cylinders in subcritical flow, *AIAA J.* **8,** 1814–1821 (1970).
14. V. Modi and A. Dikshit, Near wakes of elliptic cylinders in subcritical flow, *AIAA J.* **13,** 490–497 (1975).
15. V. Modi and L. Ieong, On some aspects of unsteady aerodynamics and vortex induced oscillations of elliptic cylinders at subcritical Reynolds number, *ASME J. Mech. Design* **100,** 354–362 (1978).
16. T. Ota, H. Nishiyama and Y. Taoka, Flow around an elliptic cylinder in the critical Reynolds number regime, *ASME J. Fluids Engng* **109,** 149–155 (1987).
17. R. Seban and R. Drake, Local heat-transfer coefficients on the surface of an elliptic cylinder in a high speed air stream, *Trans. Am. Soc. Mech. Engrs* **75,** 235–240 (1953).
18. R. Drake, R. Seban, D. Doughty and S. Lin, Local heat-transfer coefficients on surface of an elliptic cylinder, axis ratio 1 : 3, in a high speed air stream, *Trans. Am. Soc. Mech. Engrs* **75,** 1291–1302 (1953).
19. T. Ota, S. Aiba, T. Tsuruta and M. Kaga, Forced convection heat transfer from an elliptic cylinder of axis ratio 1 : 2, *Bull. Japan Soc. Mech. Eng.* **26,** 262–267 (1983).
20. T. Ota, H. Nishiyama and Y. Taoka, Heat transfer and flow around an elliptic cylinder, *Int. J. Heat Mass Transfer* **27,** 1771–1779 (1984).
21. H. Nishiyama, T. Ota and T. Matsuno, Forced convection heat transfer from two elliptic cylinders in a tandem arrangement, *Trans. Japan Soc. Mech. Eng.* **52B,** 2677–2681 (1986).
22. H. Nishiyama, T. Ota and T. Matsuno, Heat transfer and flow around elliptic cylinders in tandem arrangement, *JSME Int. J. Series II* **31,** 410–419 (1988).
23. V. Ilgarubis, R. Ulinskas and A. Butkus, Hydraulic drag and average heat transfer coefficients of compact bundles of elliptical finned tubes, *Heat Transfer—Soviet Res.* **20,** 12–21 (1988).
24. E. Eckert, Die Berechnung des warmeubergangs in du laminaren grenzschicht umstromter korper, *VDI ForschHft.* **13,** 1–44 (1942).
25. B. Chao and R. Fagbenle, On Merk's method of calculating boundary layer transfer, *Int. J. Heat Mass Transfer* **17,** 223–240 (1974).
26. J. Merkin, Free convection boundary layers on cylinders of elliptic cross section, *ASME J. Heat Transfer* **99,** 453–457 (1977).
27. H. M. Badr, A theoretical study of laminar mixed convection from a horizontal cylinder in a cross stream, *Int. J. Heat Mass Transfer* **26,** 639–653 (1983).
28. P. K. G. Panniker and Z. Lavan, Flow past impulsively started bodies using Green's functions, *J. Computational Phys.* **18,** 46–65 (1975).
29. H. M. Badr and S. C. R. Dennis, Time-dependent viscous flow past an impulsively started rotating and translating circular cylinder, *J. Fluid Mech.* **158,** 447–486 (1985).
30. H. M. Badr, S. C. R. Dennis, M. Coutanceau and C. Menard, Unsteady flow past a rotating circular cylinder at Reynolds numbers 10^3 and 10^4, *J. Fluid Mech.* **220,** 459–484 (1990).
31. A. N. Staniforth, Studies of symmetrical and asymmetrical viscous flows past impulsively started cylinders, Ph.D. dissertation, Dept. Appl. Math., University of Western Ontario (1972).
32. A. P. Hatton, D. D. James and H. W. Swire, Combined forced and natural convection with low-speed air flow over horizontal cylinders, *J. Fluid Mech.* **42,** 17–31 (1970).
33. D. C. Collis and M. J. Williams, Two-dimensional convection from heated wires at low Reynolds numbers, *J. Fluid Mech.* **6,** 357–384 (1959).
34. S. C. R. Dennis, J. D. Hudson and N. Smith, Steady laminar forced convection from a circular cylinder at low Reynolds number, *Phys. Fluids* **11,** 933–940 (1967).